RESEARCH



Nonlinear optical properties of Azo compound synthesized via diazonation reaction using continuous wave laser beams

M. J. Ashoor¹ · Sadiq M. H. Ismael² · Hanadi M. Jarallah² · H. A. Sultan¹ · Qusay M. A. Hassan¹ · Kawkab Ali Hussein² · C. A. Emshary¹

Received: 16 September 2024 / Accepted: 23 February 2025 © The Author(s), under exclusive licence to Springer-Verlag GmbH Germany, part of Springer Nature 2025

Abstract

In the presence of nitrite and an aqueous hydrochloric acid medium, sulfadiazine is diazonated to create an azo compound. With the chemical formula (E)-4-((3- (tert-butyl)-2-hydroxy-5-methoxyphenyl) diazenyl)-N-(pyrimidin-2-yl), the compound is a synthetic benzenesulfonamide. Characterization of the azo molecule is done using mass, FTIR, and ^{1}H and ^{13}C NMR spectra. Azo compound structure is optimized using Density Functional Theory (DFT). This study examines the nonlinear optical (NLO) characteristics of the azo compound via the utilization of two visible, continuous wave (CW) laser beams. The nonlinear refractive index (NLRI) and the nonlinear absorption coefficient (NLAC) of the azo compound are estimated using diffraction patterns (DPs) and Z-scan and found equal to 5.38×10^{-7} cm²/W and 2.03×10^{-3} cm/W, respectively. The DPs are numerically simulated using the Fraunhofer approximation of the Fresnel-Kirchhoff integral with good accord compared to the experiment's findings. The all-optical switching (AOS) behavior of the azo compound is examined under irradiation with 473 and 532 nm CW laser beams.

1 Introduction

Over the last four decades, there has been a continuing increasing interest in the development of new materials that can be used with low-intensity, continuous wave (CW) laser beams for possible use in optical switching [1], optical limiting [2], optical information processing [3], harmonic generation [4], and optical computing [5]. Many classes of materials, such as organic materials [6], organometallics [7], inorganic materials [8], and fullerenes [9] are extensively explored. In the last four years, we have investigated the linear and nonlinear properties of a large number of materials [10–22]. Azo compounds are another group of materials whose nonlinear optical (NLO) properties have been investigated thoroughly [23–31]. During the period 1965–1990, three techniques viz., thermal lens (TL) [32], diffraction patterns (DPs) [33, 34], and Z-scan [35, 36], have been developed to measure the nonlinear refractive index (NLRI), n₂,

Qusay M. A. Hassan qusayali64@yahoo.co.in

Published online: 09 March 2025

and the change of refractive index, Δn . The Z-scan (closed and open) developed by Sheik Bahae et al. [35, 36] is a simple and effective tool used to measure NLRI of so many materials, together with magnitudes of the real and imaginary parts of the nonlinear susceptibility and the sign of the real part. These two parameters are obtained via the closed aperture (CA) Z-scan, while the nonlinear absorption coefficient (NLAC), β , obtained using the open aperture (OA) Z-scan.

The presence of azo (-N=N-), which conjugates the two aromatic rings, gives azo compounds their vibrant color [37, 38]. These compounds have gained massive attraction owing to their versatile biological such as, antimicrobial [39, 40], and anticancer [41], as well as industrial applications, electronic devices [42], sensors [43], and fluorescent probes [44]. The azo aromatic compounds are used in the field of nonlinear optics, optical data storage and their optical and spectroscopic properties [45–48]. The electronic and structural properties of materials can be identified by using quantum chemical calculation techniques [49, 50]. Density functional theory (DFT) study was used to analyze the localization of the highest occupied molecular orbital (HOMO) – and the lowest unoccupied molecular orbital (LUMO).

The aim of the current study is to find a new material that possesses high nonlinear optical (NLO) properties.



Department of Physics, College of Education for Pure Sciences, University of Basrah, Basrah 61001, Iraq

Department of Chemistry, College of Education for Pure Sciences, University of Basrah, Basrah 61001, Iraq

71 Page 2 of 27 M. J. Ashoor et al.

Therefore, in this research, we synthesized a novel azo compound and characterized it via mass spectrometry, Fourier transform infrared spectroscopy (FTIR), and both ¹H and ¹³C nuclear magnetic resonance (NMR) spectroscopy. The NLO properties of the azo compound were investigated under irradiation with a continuous wave (CW) laser beam at 473 nm. Utilizing diffraction patterns (DPs) and the Z-scan techniques, we have measured the compound's nonlinear refractive index (NLRI) and nonlinear absorption coefficient (NLAC). Additionally, all-optical switching (AOS) technique were discovered with two laser beams at 473 and 532 nm.

2 Experimental

2.1 Synthesis of (E)-4-((3-(tert-butyl)-2-hydroxy-5 -methoxyphenyl) diazenyl)-N-(pyrimidin-2-yl) benzenesulfonamide, (compound A)

An ice bath was used to cool a 1.251 g, 5 mmol sulfadiazine solution that was submerged in a diluted hydrochloric acid (HCl) solution (concentrated HCl: $\rm H_2O$, 1:1 v/v) at temperatures lower than 5 °C. Drop by drop, NaNO2 (0–38 g) dissolved in 10 mL of distilled water was added in relation to the prior material. This mixture, dipped in an ice bath, was constantly swirling. At a concentration of 5 mmol, 0.901g of tert-butyl-4-hydroxyanisole was added gradually to the mixture mentioned above. The resulting liquid was cooled in an

Fig. 1 AOS experimental set up

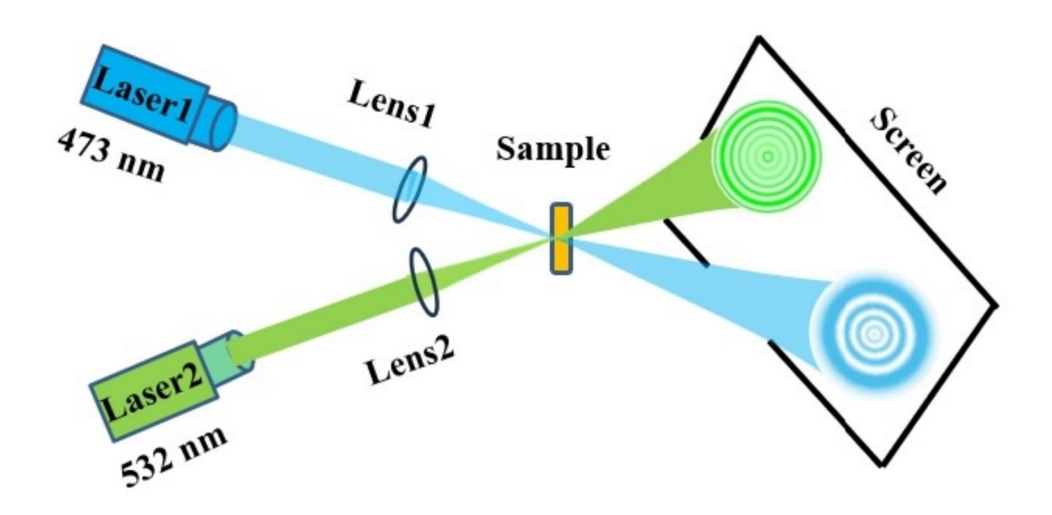


Fig. 2 Synthesis routes of azo compound

$$\begin{array}{c|c}
 & O \\
 & N \\
 & N \\
 & N \\
 & O
\end{array}$$

$$\begin{array}{c|c}
 & O \\
 & N \\
 & N \\
 & O
\end{array}$$

$$\begin{array}{c|c}
 & O \\
 & N \\
 & N \\
 & O
\end{array}$$

$$\begin{array}{c|c}
 & O \\
 & N \\
 & N \\
 & O
\end{array}$$

$$\begin{array}{c|c}
 & + & - \\
 & N \\
 & N \\
 & O
\end{array}$$

$$\begin{array}{c|c}
 & + & - \\
 & N \\
 & N \\
 & O
\end{array}$$

$$\begin{array}{c|c}
 & + & - \\
 & N \\
 & N \\
 & O
\end{array}$$

$$\begin{array}{c|c}
 & + & - \\
 & N \\
 & N \\
 & O
\end{array}$$

Diazonium Salt



ice bath and stirred for a duration of 35 min. Subsequently, the resulting powder was filtered and subjected to further dealing out using ethanol. Finally, the desired product was evaporated for 24 h in an oven set at 50 °C. Yield of dark red solid, melting point 195–197 °C: 79%. IR spectra showing 3433 (OH), 1583 (aromatic C=C), 1492 (N=N), and 1163–1354 (C–O) at H cm⁻¹. The chemical formulas are as follows: 1.41 (s, 9H, t-But), 3.75 (s, 3H, OCH₃), 11.27 (s, 1H, NH), 12.01 (s, 1H, OH), and 7.02–8.56 (m, 9H, Ar–H). The MS [EI] + m/z value is 441.3 [M]+.

2.2 Experimental setup

A Gaussian CW laser beam of wavelength 473 nm was used as the illumination beam. The laser beam spot size as it leaves the laser device output coupler equals 1.5 mm (at e^{-2}) when focused by a 5 cm focal length lens to a spot size of 19.235 μm . A sample glass cell of 1 mm thickness was placed at the lens focus, and the transmitted laser beam was projected onto an observation 30×30 cm semitransparent screen, which was placed 85 cm from the sample cell. The resulted DPs were recorded by a digital camera.

The Z-scan experiments were performed using the 473 nm laser beam, which was focused by 5 cm focal length

lens. The Rayleigh length of the beam equals 2.456 mm. The same sample cell was used before in these experiments. The intensity of the transmitted beam through the sample was measured in the far field with the closed aperture (CA) Z-scan technique using a photo detector covered with a 2 mm iris. For the open aperture (OA) Z-scan, a lens replaced the aperture to collect the entire laser beam transmitted through the sample.

The all-optical switching (ASO) experiments depicted in Fig. 1 employ two laser beams: the controlling beam with a wavelength of 473 nm and the controlled beam with a wavelength of 532 nm. The absence of rings in the sample cell can be attributed to the low absorption coefficient of the medium at the 532 nm beam so that small amount of energy is absorbed. When the beam with the wavelength 473 nm traverses the same medium with a high absorption coefficient, a substantial amount of energy is absorbed, leading to the formation of rings, even with a moderate power input. When both beams pass through the medium via the cross-passing technique [51–53], two types of DPs appeared, one for each beam.

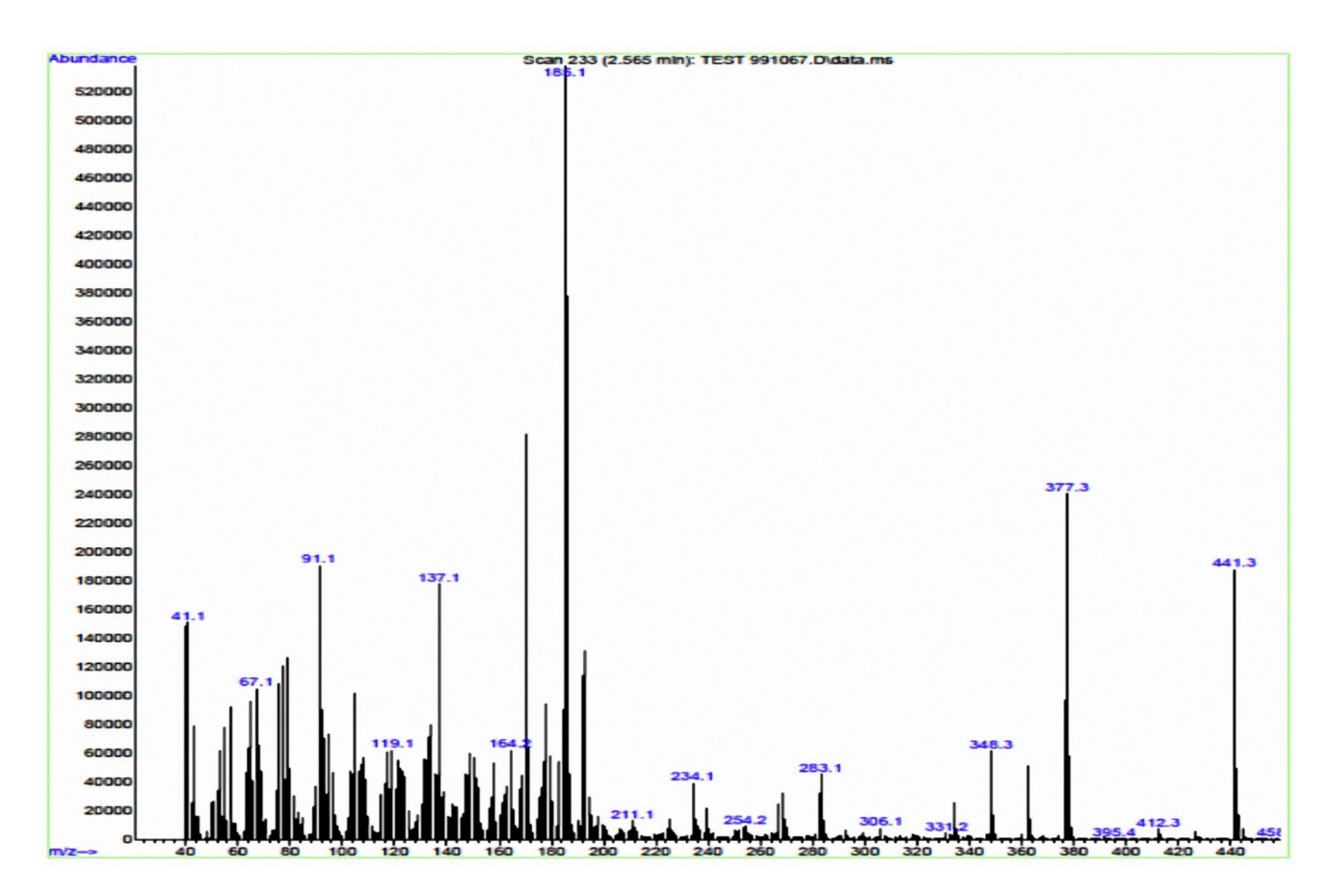


Fig. 3 Mass spectrum of azo compound



71 Page 4 of 27 M. J. Ashoor et al.

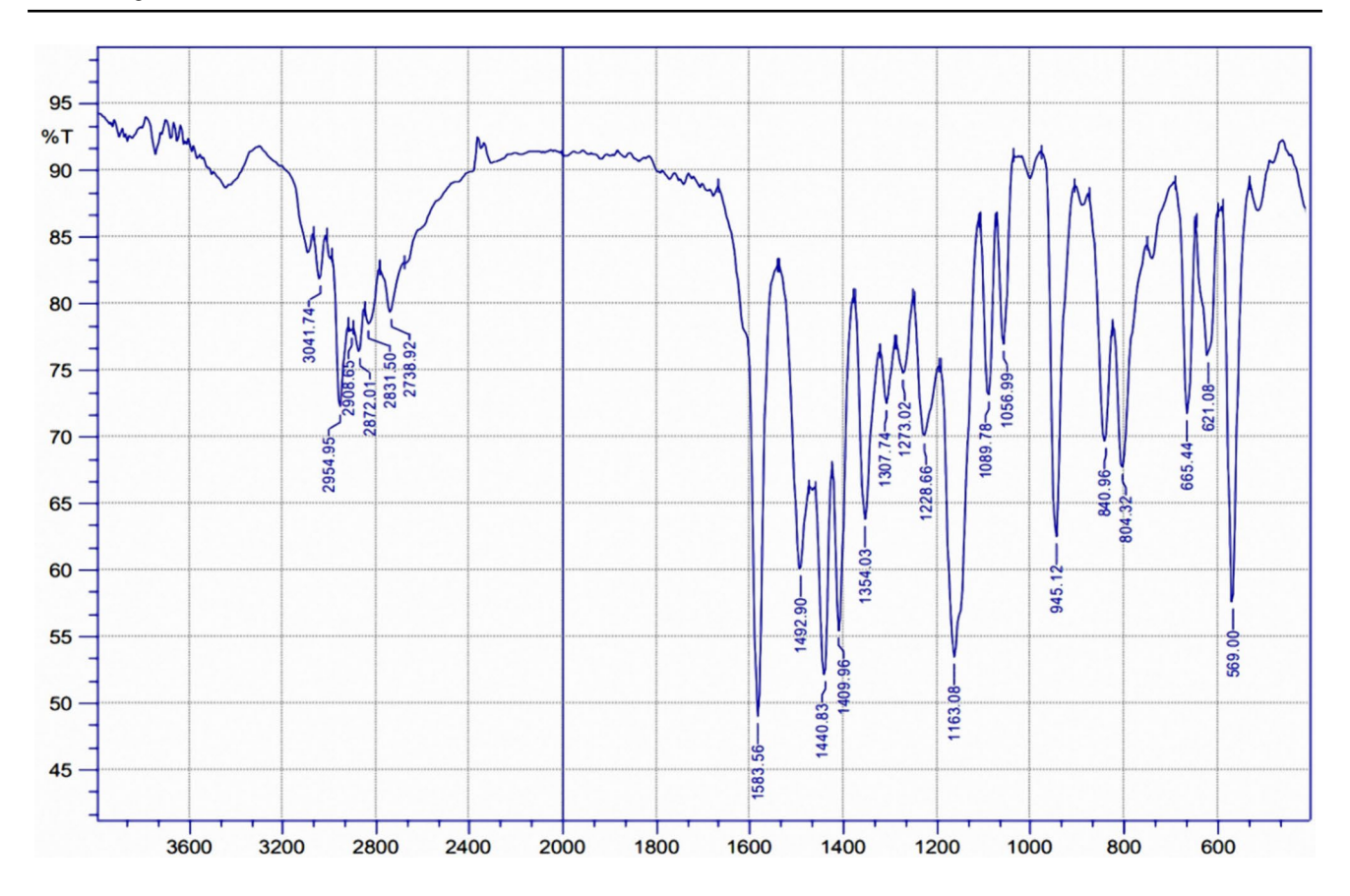


Fig. 4 FT-IR spectrum of azo compound

3 Results

3.1 Chemistry

The present study includes the synthesis of diazonium salts via the diazonation reaction of sulfadiazine using sodium nitrite and an aqueous sulfuric acid (HCl). Figure 2 illustrates the synthesis of azo compound from novel diazonium compound with 3-tert-butyl-4-hydroxyanisole.

The structure was verified through mass spectrometry, ¹H NMR, and infrared spectroscopy. As illustrated in Fig. 3, the mass spectrum analysis of the azo compound reveals a molecular ion peak at m/z 441.3. The FT-IR spectrum shows significant absorption bands corresponding to the v(C-O) group within the range 1163–1354 cm⁻¹. The bands attributed to v(N=N) and aromatic C=C stretching are observed at 1492 cm⁻¹ and 1583 cm⁻¹, respectively. Additionally, the band at 3433 cm⁻¹ is identified as v(OH) phenolic, as depicted in Fig. 4. Due to the interaction between the donor and acceptor electrons, the intermolecular charge transfer (ICT) increases in the conjugated molecular structure, resulting in large NLO properties. On the other hand, several C=C stretching modes are created as a result of the ICT process, and this gives rise to the

ICT process via the p-system. Several medium and strong bands at 1570, 1458 and 1442 cm⁻¹ in the spectrum are assigned to C=C stretching vibrations in the current work. This frequency confirms that the dye molecule is highly polarized, which improves the NLO properties [54]. The ¹H NMR spectrum of the azo compound reveals the following chemical shifts: a singlet at 1.41 ppm, representing 9 protons from the tert-butyl group; a singlet at 3.75 ppm, corresponding to 3 protons from the methoxy group; a singlet at 11.27 ppm, assigned to 1 proton from the amine group; and a singlet at 12.01 ppm, attributed to 1 proton from the hydroxyl group. Aromatic protons are observed as several signals in the range $\delta = 7.02-8.56$ ppm (9H, Ar–H), with additional singlets at $\delta = 11.27$ ppm (1 proton, NH) and $\delta = 12.01$ ppm (1 proton, OH). Data from the ¹H NMR spectrum is displayed in Fig. 5. Additionally, the ¹³CNMR spectrum data is shown in Fig. 6. The signal detected at $\delta = 35.27$ ppm is ascribed to the carbon atom present in the t-Butyl group. At 55.79 ppm, the characteristic peak is caused by the carbon atom in the methoxy group. The chemical shifts of the identified aromatic carbons range from 123.22 to 152.47 ppm [55].



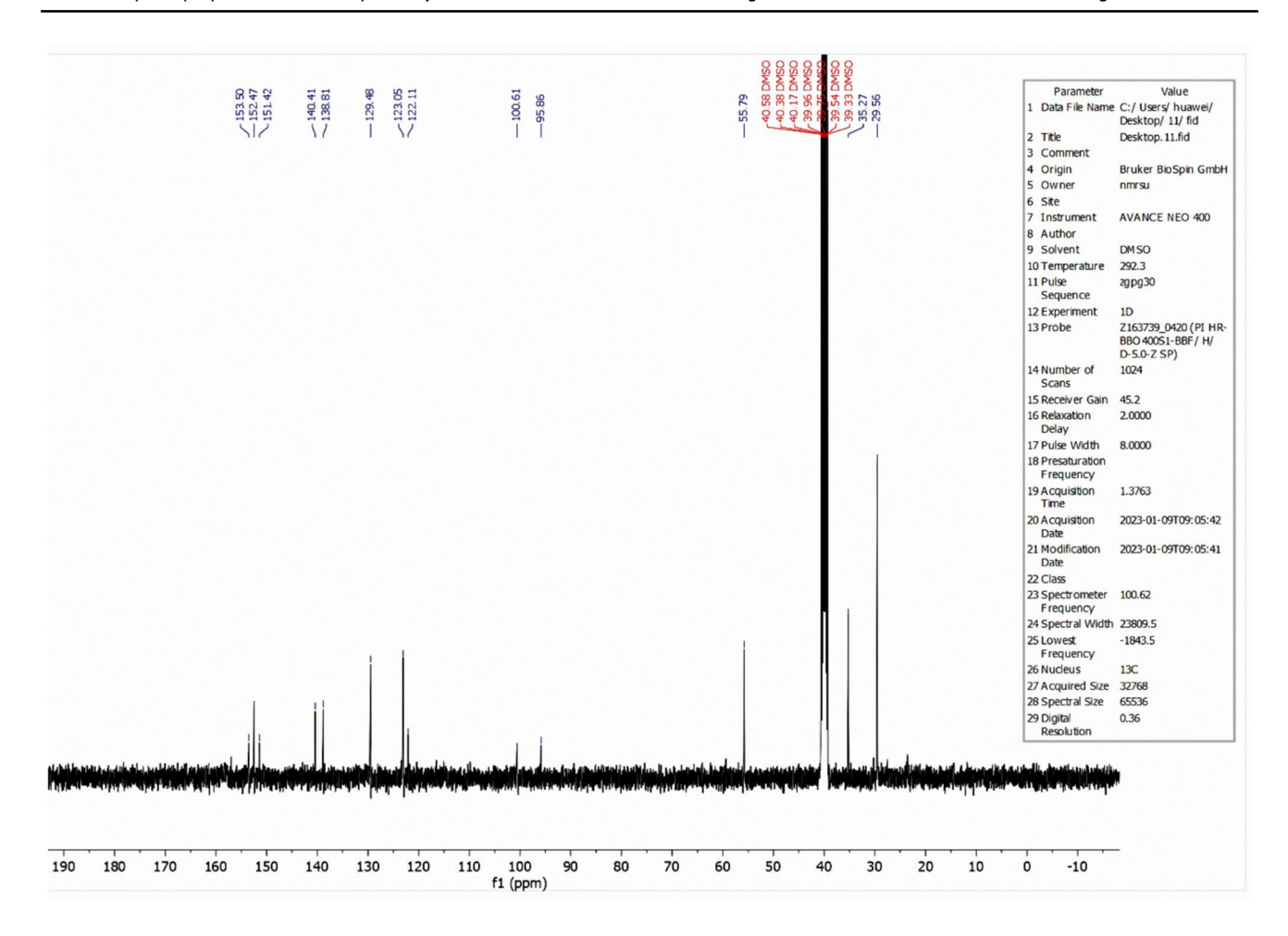


Fig. 5 ¹H NMR spectrum of azo compound

3.2 Density functional theory study

The program Gaussian 09 [56] was used to find the geometrical structure for the minimum energy of the structure. The geometrical structure was optimized using the DFT/B3LYP approach with a 6–311+G(d,p) basis set level. DFT calculations of several chemical quantum descriptors (CQDs), such as the HOMO, the LUMO energies, and energy gap, were calculated to better understand the geometrical characteristics, stability, and electronic properties of the azo compound [57, 58] are listed in Table 1.

The evaluation of particular aspects of physical chemistry, structure, and nonlinear behaviors was done theoretically. The stability can be determined using the CQD data obtained through DFT calculations. A molecule's size, shape, electrostatic potential (including electrons and nuclei), and molecular structure are all represented graphically by a molecular electrostatic potential surface (MEP). In addition, it provides a visual representation of the relative polarization. Indeed, it is quite advantageous in the

examination of the correlation between physicochemical characteristics and molecular structure. Contour maps for positive and negative electrostatic potentials for the azo compound are shown in Fig. 7.

3.3 Spectroscopic analyses of the A-OCH₃ compound

Three absorption bands were visible in the azo compound's UV–visible spectrum. The first peak, seen at the wavelength of 263 nm ($\lambda 1$), is ascribed to the (π – π *) transition of the aromatic rings (C=C). The absorption of the carbonyl group (C=O) is responsible for the second band, which is visible at wavelength 343 nm ($\lambda 2$) and is linked to the (π - π *) transition. The absorption bands observed at wavelength 343 nm ($\lambda 3$) can be attributed to the (π - π *) transitions of the azomethine group (C=N) (Fig. 8). And then the UV–vis. By computing vertical absorptions, the spectrum was computed using the TD-DFT/B3LYP/6-311G+(d,p) level. The



71 Page 6 of 27 M. J. Ashoor et al.

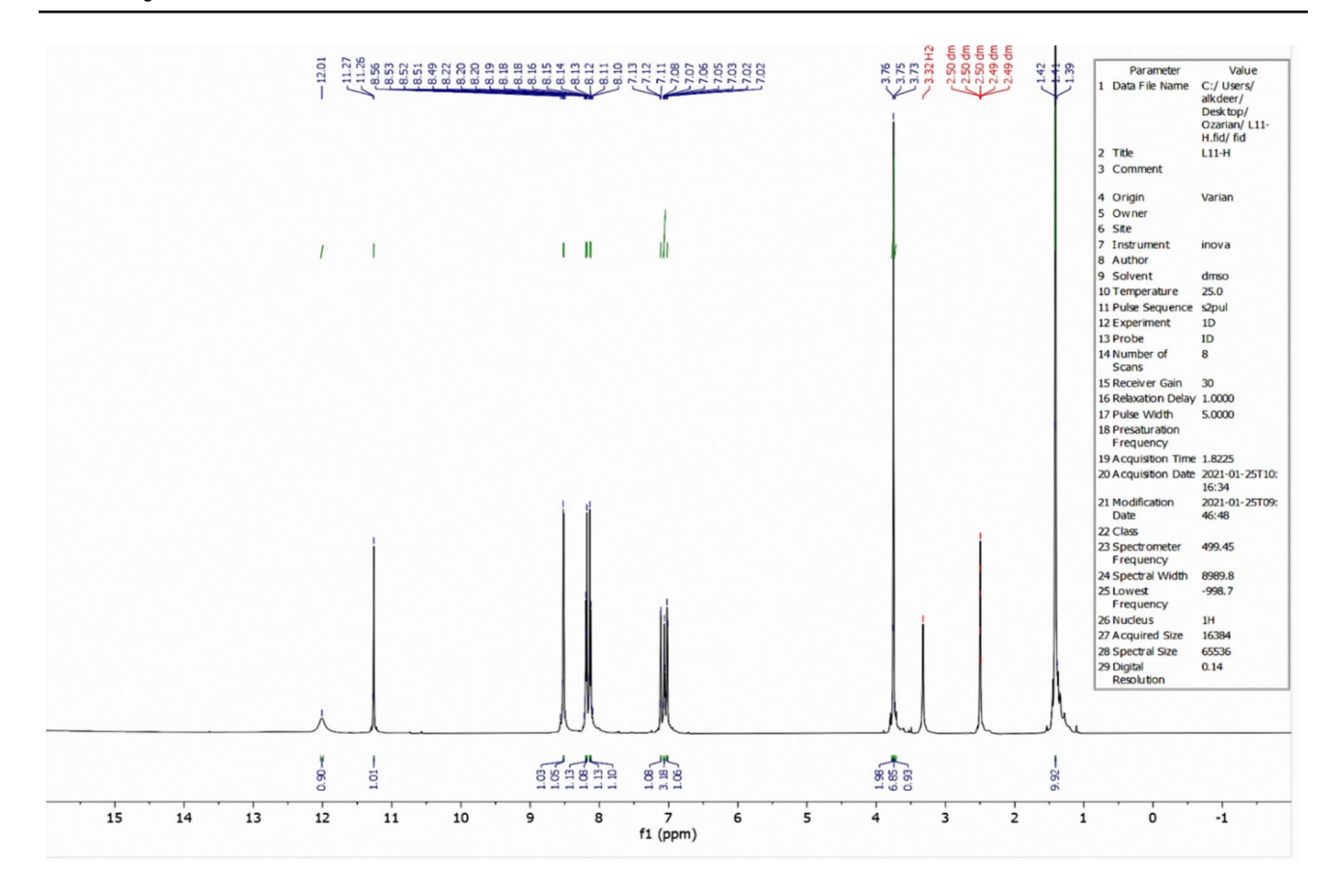


Fig. 6 ¹³C NMR spectrum of azo compound

Table 1 The azo compound's theoretically excited states

The chemical global reagent descriptors (CGRDs)	A	Urea	US	pNA	2M4NA
HOMO (eV)	-5.926	-7.379	-8.092	-8.4703	-6.5279
LUMO (eV)	-3.039	-0.362	-0.611	-0.5137	-2.4141
Egap (eV)	2.887	7.016	7.480	7.9565	4.1138
Dipole moment μ (Debye)	6.683	3.885	4.7512	7.482	7.6494
Polarizability (α) (a.u)	377698	33.802	74.4066	101.802	114.595
Hyper polarizability (β) (a.u)	3224.532	71.518	64.7518	1660.83	1664.702
$E_{opt}(eV)$	2.428	_	_	_	_
E _b (eV)	0.459	-	-	-	_

calculations for the excited states of the azo compound are presented in Table 2.

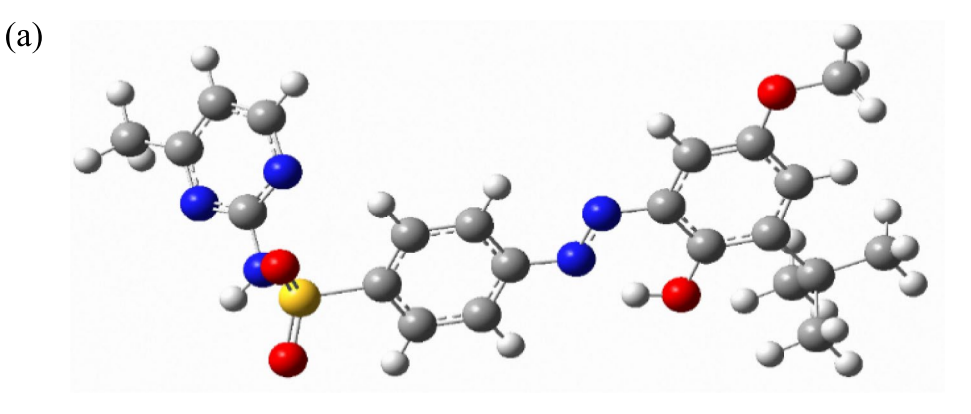
The estimated UV–vis. is displayed in Fig. 9. However, in the gas phase, absorptions were found at wavelengths of 430.88 nm (λ 1), 317.08 nm (λ 2), 327.32 nm (λ 3), 355.45 nm (λ 4), 465.43 nm (λ 5), and 510.6 nm (λ 6) [59, 60]. Overall, the experimental and DFT study of UV–vis. absorption spectra results were inconsistent since the calculations were performed in a gaseous solution.

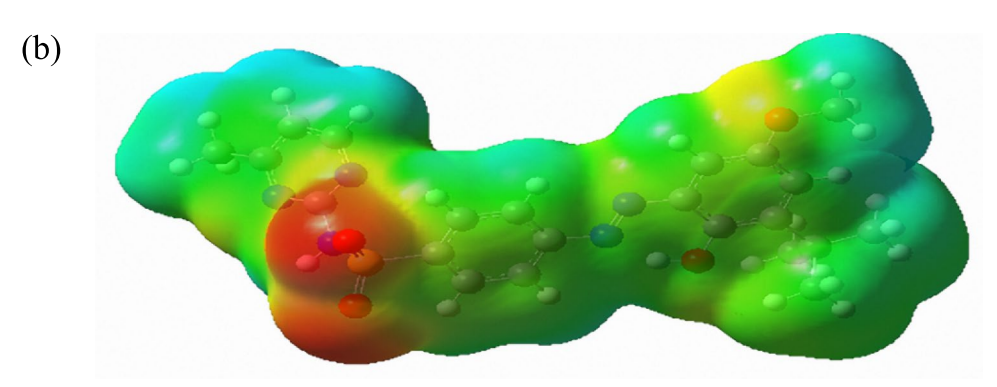
Despite the discrepancy between experimental and theoretical data, the UV-vis., and the TD-DFT method's prediction results agree satisfactorily with the experimental data. The azo compound's absorption spectra are displayed in Fig. 10, where the oscillator strength is compared to the gas phase wavelength. At a magnitude of 0.775, the oscillation reaches its maximum wavelength of 355.44 nm [61].

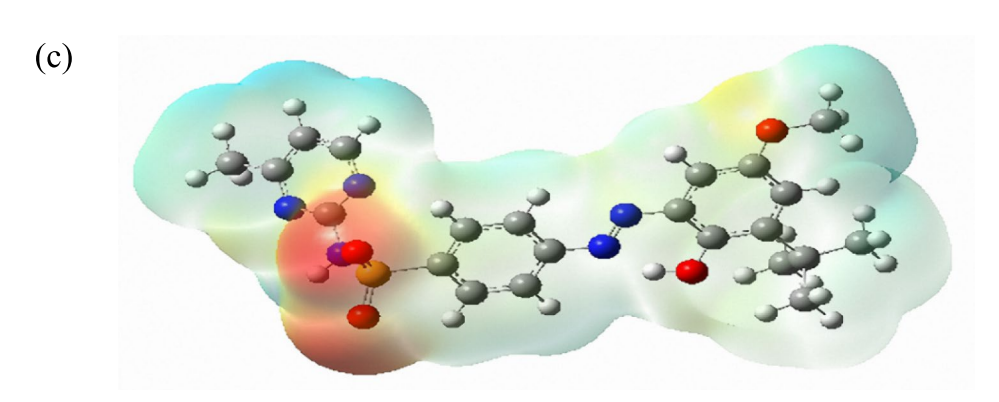
The linear absorption coefficients, α , of the azo compound at wavelengths 473 and 532 nm are 18.42 cm⁻¹ and

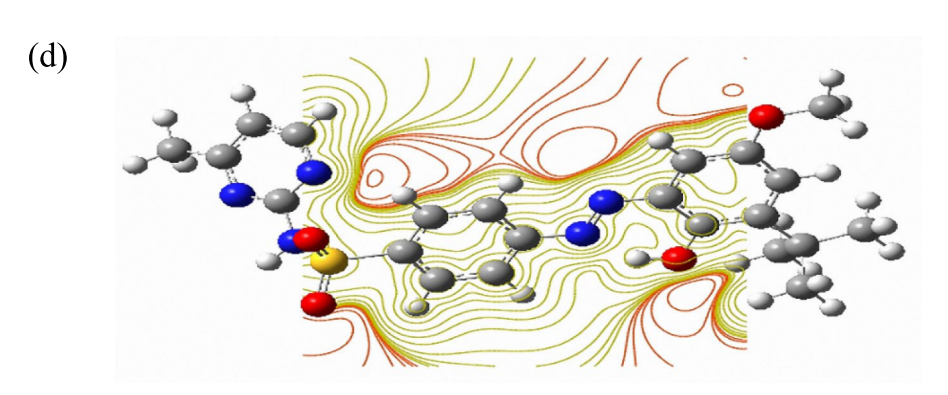


Fig. 7 a Geometry optimization; b the molecular electrostatic potential (MEP) surface; and c, d maps of the azo compound's 2D and 3D iso-surfaces. The blue and red represent the positive and negative components, respectively









71 Page 8 of 27 M. J. Ashoor et al.

Fig. 8 The experimental UV–vis. absorption spectrum of the investigated azo compound

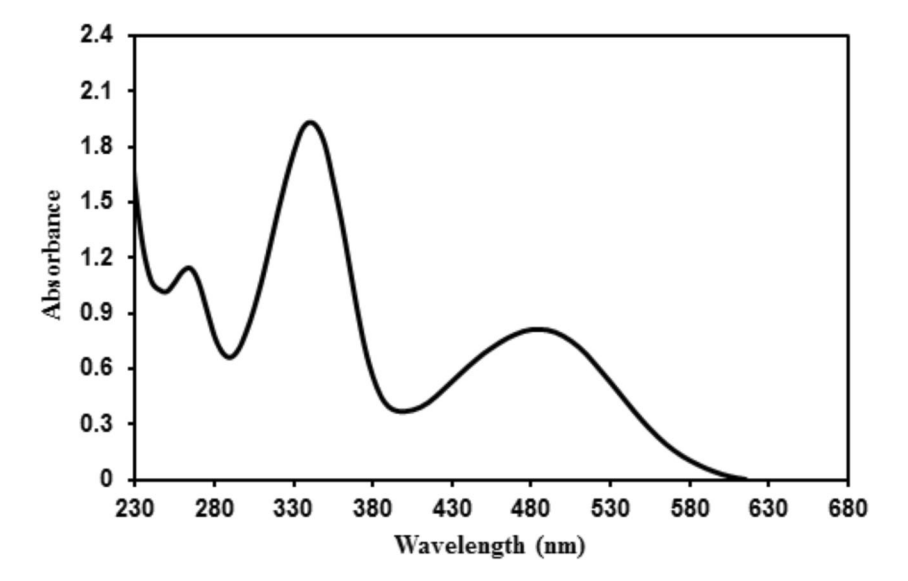
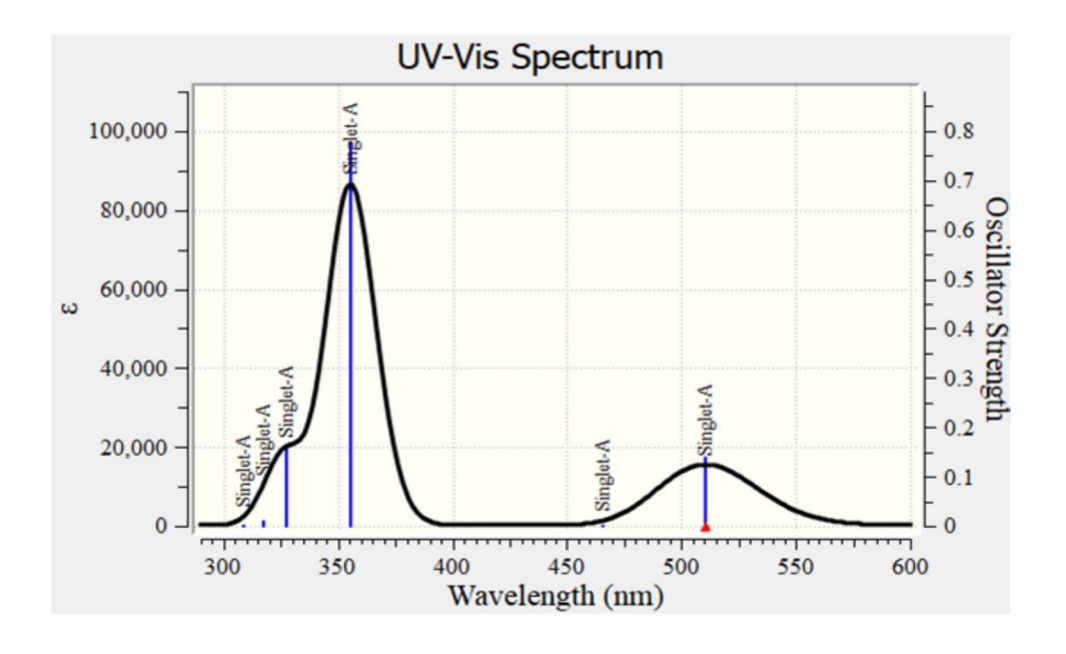


Table 2 HOMO, LUMO and CQDs calculated for azo compound

The chemical global reagent descriptors (CGRDs)	A	Urea	US	pNA	2M4NA
HOMO (eV)	- 5.926	-7.379	-8.092	-8.4703	-6.5279
LUMO (eV)	-3.039	-0.362	-0.611	-0.5137	-2.4141
Egap (eV)	2.887	7.016	7.480	7.9565	4.1138
Dipole moment μ (Debye)	6.683	3.885	4.7512	7.482	7.6494
Polarizability (α') (a.u)	377698	33.802	74.4066	101.802	114.595
Hyper polarizability (β) (a.u)	3224.532	71.518	64.7518	1660.83	1664.702
$E_{opt}(eV)$	2.428	_	_	_	_
$E_b(eV)$	0.459	_	-	-	_

Fig. 9 Theoretical spectrum calculated by TD-DFT/B3LYP/6–311+G(d,p) of azo compound





Osc. Strength (f) vs Wavelength (nm)

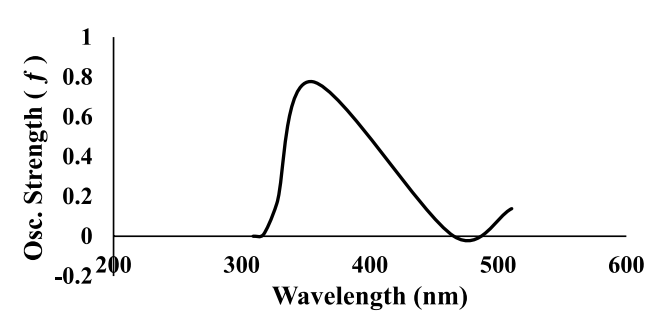


Fig. 10 Simulated oscillator strength (f) against wavelength (nm) in the gas phase of azo compound

10.91 cm⁻¹, respectively, which were calculated using the equation mentioned in a previous study [62] and Fig. 8.

Table 2 displays the parameters of quantum chemistry. A potential electron acceptor is the LUMO, whereas a potential electron donor is the HOMO [63]. The closing charge transfer interaction inside the molecule is described by the HOMO-LUMO energy gap (ΔE), which is helpful in identifying the molecular electrical transport features. A high ΔE molecule has a low level of chemical reactivity and a large kinetic stability [64]. According to the ΔE value of [6.6] phenyl-C61-butyric acid methyl ester (PCBM) determined by B3LYP/B3LY/6-31G*, the ΔE of the investigated molecule (2.887 eV) is large [65]. Furthermore, a low ΔE value suggests that the molecule is more likely to undergo electronic changes, which raises the possibility that it will exhibit NLO activity. Based on Table 2, the azo compound has a narrower ΔE than pNA, 2M4NA, and urea-sulphamic acid. The azo compound exhibits

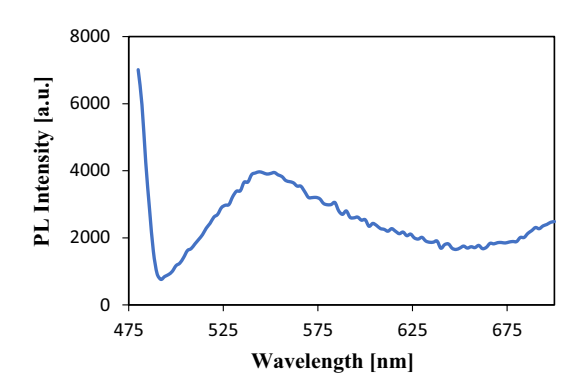


Fig. 12 Photoluminescence spectrum of the azo compound in DMF solvent

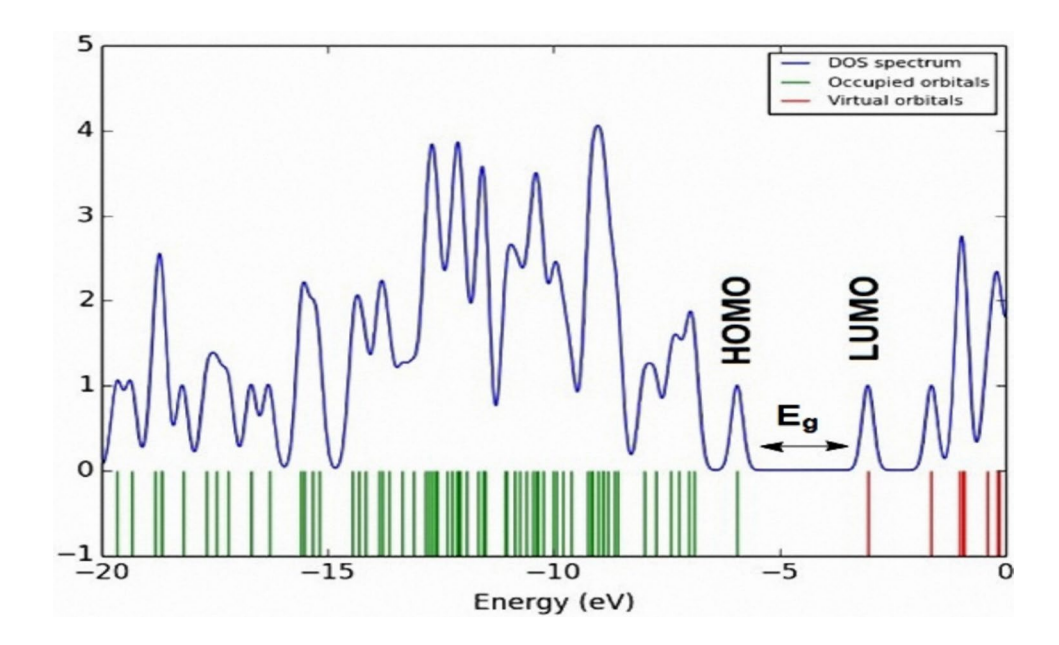
stronger polarizability (α') values compared to urea [66], urea-sulphamic [67], pNA [68], and 2M4NA [69]. The presence of significant intermolecular charge transfer (ICT) within the molecule indicates a NLO response. The α' and β values of the azo molecule are higher than those of the reference substances. The general study's findings suggest that the azo compound under research has NLO features.

Binding energy, which is the difference between the energies of the electrical and optical bandgaps, is widely used method for identifying the optoelectronic characteristics of the compounds under study. It is possible to calculate the binding energy using Eq. (1) [70].

$$E_b = E_{H-L} - E_{opt} \tag{1}$$

where E_{opt} is the first excitation energy, $E_{H\text{-}L}$ is the band gap energy ΔE , and E_b is the binding energy. Materials with

Fig. 11 The frontier orbitals of the azo compound calculated at DFT/B3LYP/6–311+G(d,p) level in the gas phase





71 Page 10 of 27 M. J. Ashoor et al.

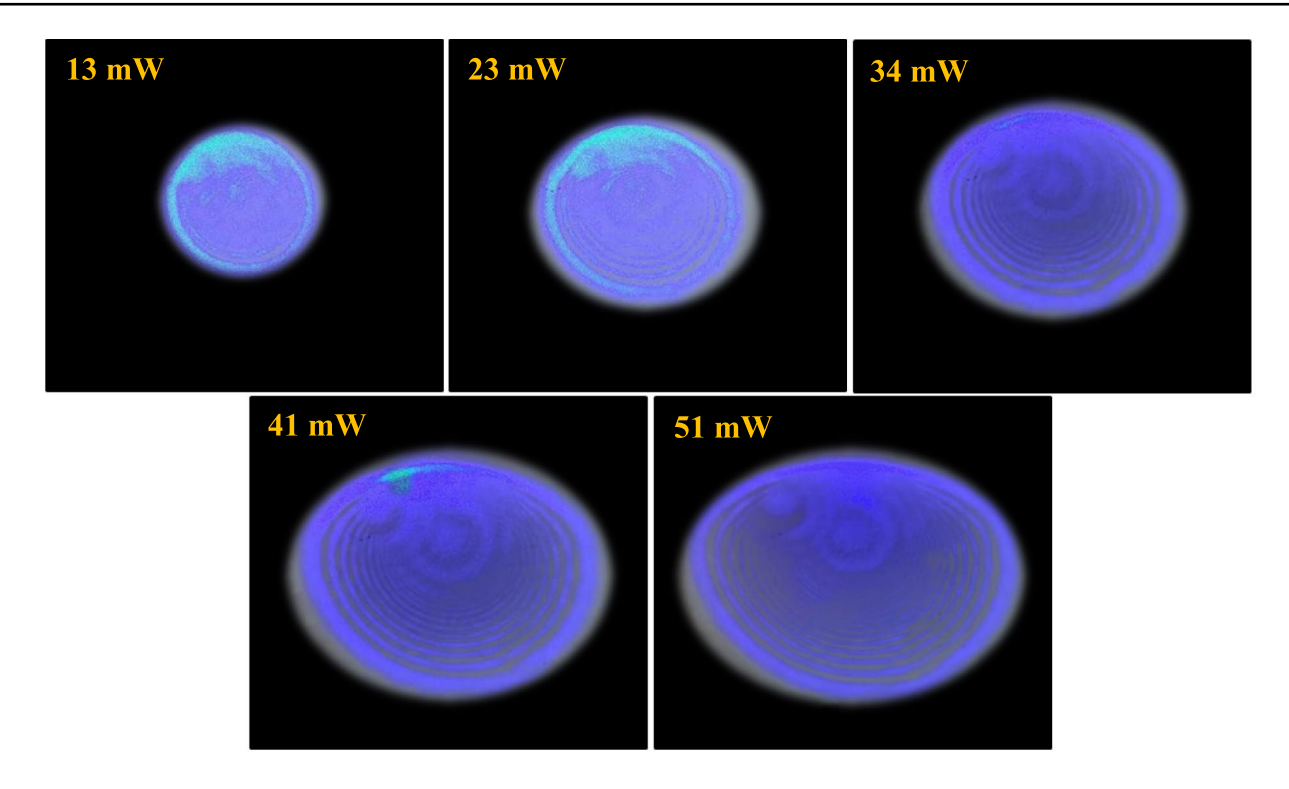


Fig. 13 Effect of power input on the DPs in the azo compound

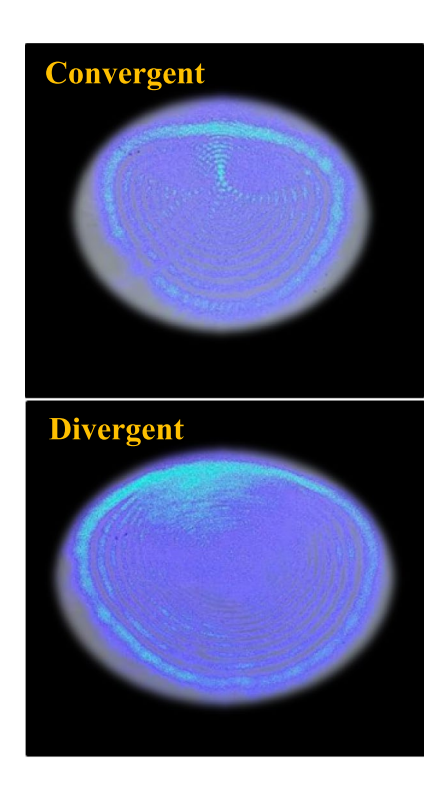


Fig. 14 Effect of type of beam wave front on the type of DPs at power input 51 mW in the azo compound



lower Eb have higher azo compound efficiency in generating electricity from absorbed light [71]. The calculated value of E_b for dye underwork is equal to 0.459 eV. It is smaller than the estimated value for PCMB that is 0.55Ev [72]. The density of states spectra for the azo compound are displayed in Fig. 11. The group contributions of HOMO and LUMO molecular orbitals were identified. The density of state (DOS) graph showed the number of orbitals that are accessible at a given energy level [73]. A decrease in the band gap is associated with an increase in conductivity since Eg is primarily capable of influencing electrical conductivity. The relationship between conductivity and Eg can be explained using Eq. (2).

$$\sigma \alpha \exp (Eg / kT)$$
 (2)

where, σ is the electrical conductivity k is the Boltzmann constant and T is the absolute temperature. This exhibits a narrowing of the band gap, Eg, which is consistent with an increase in electrical conductivity [74]. Like this, DOS spectra may also represent the creation of novel states that are to blame for the reduction in Eg [75]. For molecules with extended π -conjugated chains, the energy gap is minor [76]. Long π -conjugated chains are characterized by relatively higher values of third-order NLO property $\chi^{(3)}$ because delocalized π -electrons freely flow along conjugated molecules

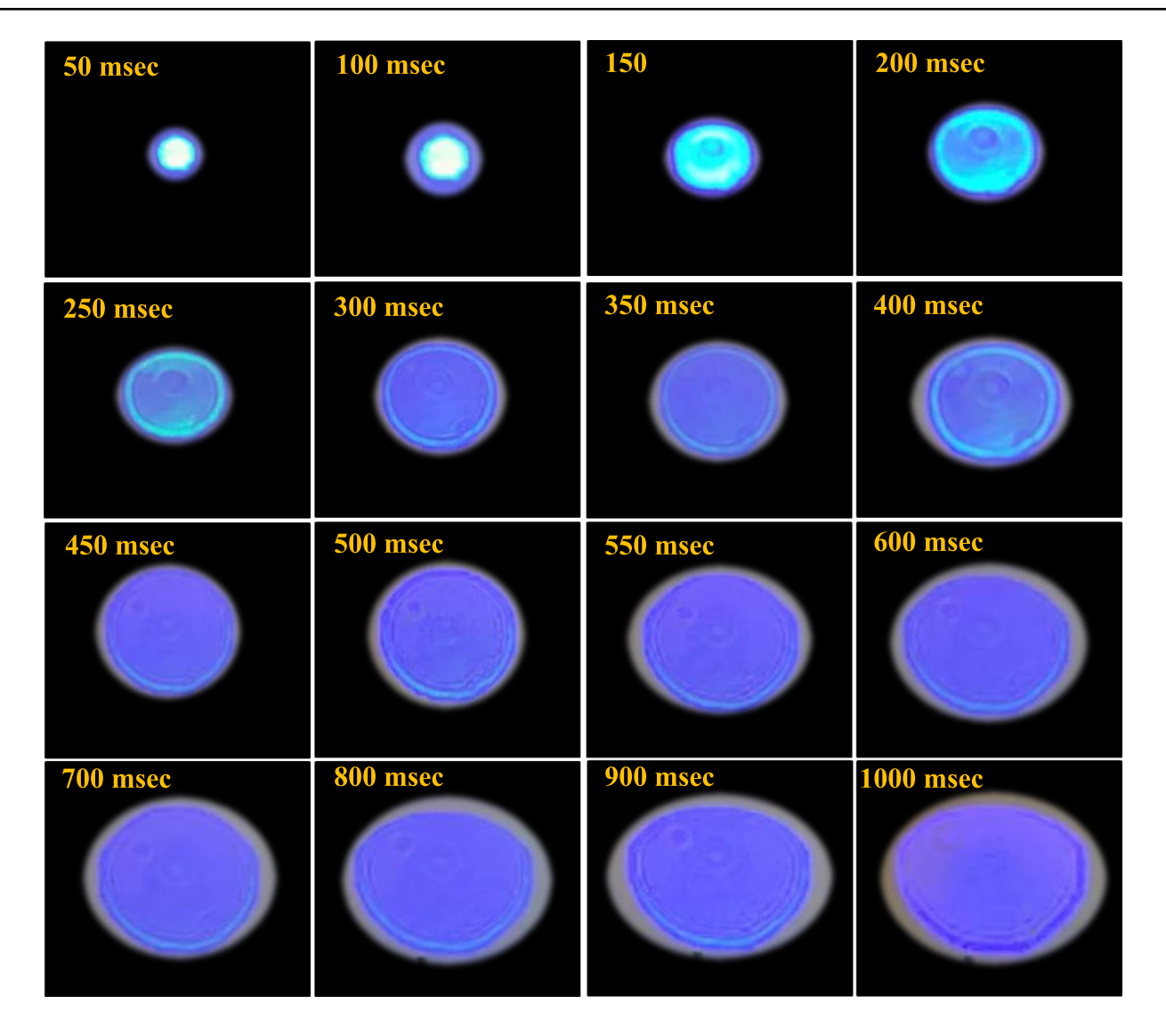


Fig. 15 Temporal evolution of a chosen DP at input power of 51 mW in the azo compound

and are the primary cause of large nonlinearities in organic materials [77].

The photoluminescence (PL) spectrum of the azo compound solution was measured using a steady-state spectrophotometer from Pico Quanta, Germany. Figure 12 presents the room-temperature PL spectrum of the azo compound solution in DMF over the wavelength range 475–700 nm. As can be seen from this figure, when the sample is excited by using a light beam at wavelength of 473 nm, the PL spectrum of the azo dye solution exhibits a abroad PL curve with a low intensity peak at a wavelength of 544 nm.

3.4 Nonlinear optical studies

Figures 13, 14 and 15 shows, respectively, the effect of slowly increasing power input of the laser beam 473 nm

traversing the sample, on the DPs, effect of the type of beam wave front on the DPs, and the temporal evolution of DPs. When the laser beam power is low, no DP appeared as a result of the small increase of the medium temperature due to the small amount of energy absorbed from the beam by the medium. With the increase of power input, the beam spot size increases, due to the self-defocusing (SDF) then it breaks into rings. The number of rings then increased and an asymmetry appeared in the upper part of the DPs. In this case, the thermal convection vertical current exceeds the thermal conduction horizontal current. When using two beams of two wavefronts types, two DPs types resulted, one for each beam, viz., divergent, and convergent.

The Z-scan experiments, viz., CA and OA were performed using the same 473 nm laser beam, which was focused using the same 5 cm focal length lens. The laser beam waist at the focus was 19.235 µm and the Rayleigh



71 Page 12 of 27 M. J. Ashoor et al.

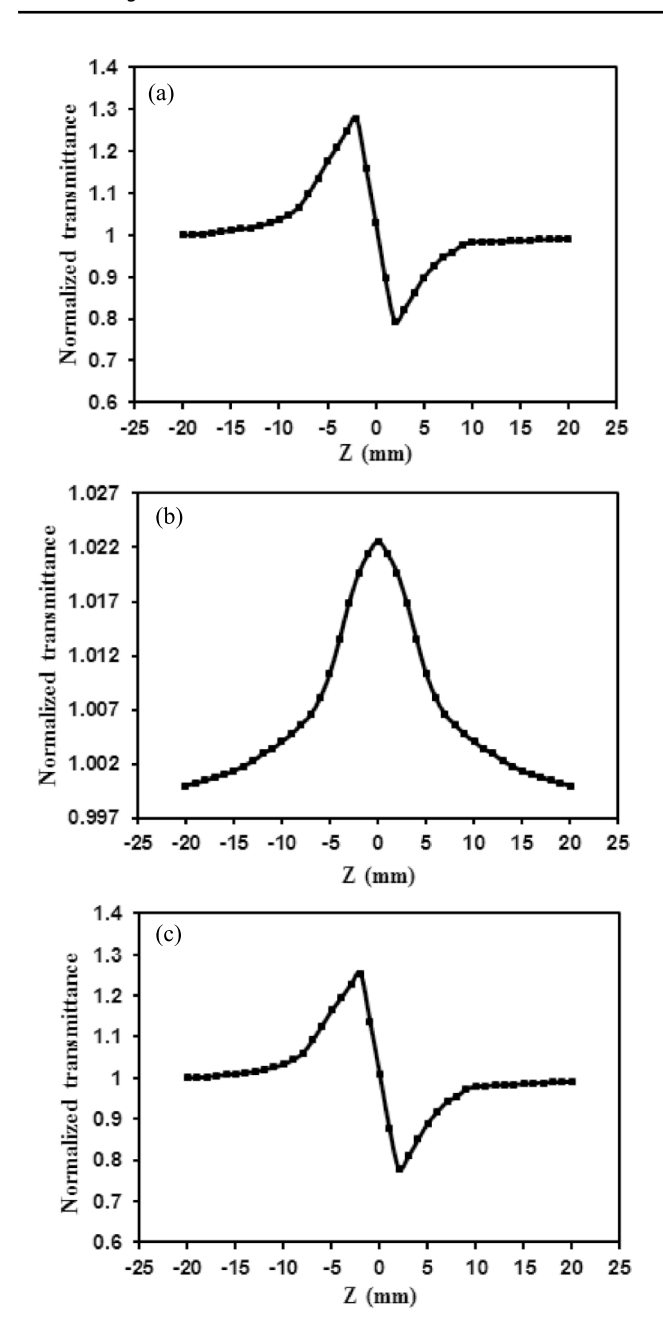
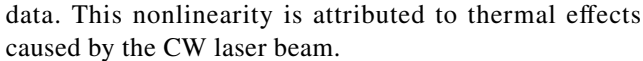


Fig. 16 Z-scan data **a** closed, **b** open and **c** division of (**a**) data by (**b**) data, at input power of 4 mW in the azo compound

length was 2.456 mm i.e., thin film criteria are satisfied since the sample cell thickness was 1 mm. Figure 16a presents the CA Z-scan data for azo compound at an input power of 4 mW. The observed peak followed by the valley in the transmittances profile indicates a negative NLRI, n_2 , signifying SDF behavior. Figure 16b illustrates the Z-scan data for the OA measurement, showing a peak at z=0, which signifies a negative NLAC, β , and indicates saturable absorption. Figure 16c displays the pure NLRI, (n_2) derived by dividing the CA Z-scan data by the OA Z-scan



In the all-optical switching experiments, two CW laser beams at 473 nm and 532 nm were employed. The 473 nm beam was used as the control, while the 532 nm beam was used as the controlled beam. Due to the low absorption coefficient of the medium at 532 nm, DPs were not observed even at high power input, whereas the high absorption coefficient at 473 nm led to distinct DPs even at moderate power input. When both beams interacted with the azo compound simultaneously, two types of diffraction patterns were produced: one for each beam even at low power input at the beam 532 nm. The control beam influenced the area, number of rings, and asymmetry of the controlled DPs, while the intensity of the DPs remained constant. The 532 nm beam controls its DPs intensity only. The 532 nm has no effect on the 473 nm DPs, In Fig. 17R1a the controlled beam draw single solid spot with no rings since the medium absorption coefficient is small and no rings appear. When the controlling beam pass through the medium DPs resulted as shown in Fig. 17R1c when both controlled and control beam pass simultaneously, two DPs types resulted as shown in Fig. 17R1 (b and c). Figure 17R2 shows the effect of the controlling beam on its DPs while Fig. 17R3 shows the effect of the controlling beam on the controlled beam DPs while the effect of the controlled beam on its DPs is shown in Fig. 17R4. This is the static AOS due to the use of two CW laser beams. By changing the 473 nm beam from CW to pulsed via connecting the laser head to the TTL function of a frequency generator while the 532 nm beam is CW, pulsed, or dynamic, AOS resulted (see Fig. 18).

3.5 Numerical simulation of the DPs

When a laser beam having Gaussian intensity profile, propagating along z-axis with its field varies in the x-y plane, where the medium has an absorption coefficient, α_{473} , at the wavelength, 473 nm, part of the beam energy is absorbed and radiated in the medium, the temperature of the medium rise locally in the shape of a Gaussian distribution. The absorption changes the medium refractive index, hence, the beam phase, $\Delta \varphi$, suffers changes. The change of the medium refractive index mimics the shape of negative (divergent) lens acts on widening the beam wave front, i.e., SDF occurs, and diffraction patterns resulted. Taking the beam field, E_o, falling on the cell and having spot size radius, ω , (at e⁻²), k is the propagation wave vector, R is the wave front radius of the beam, and P is the beam power falling on the sample cell, so that the beam complex amplitude at the entrance of the medium can be written as follows [78]:



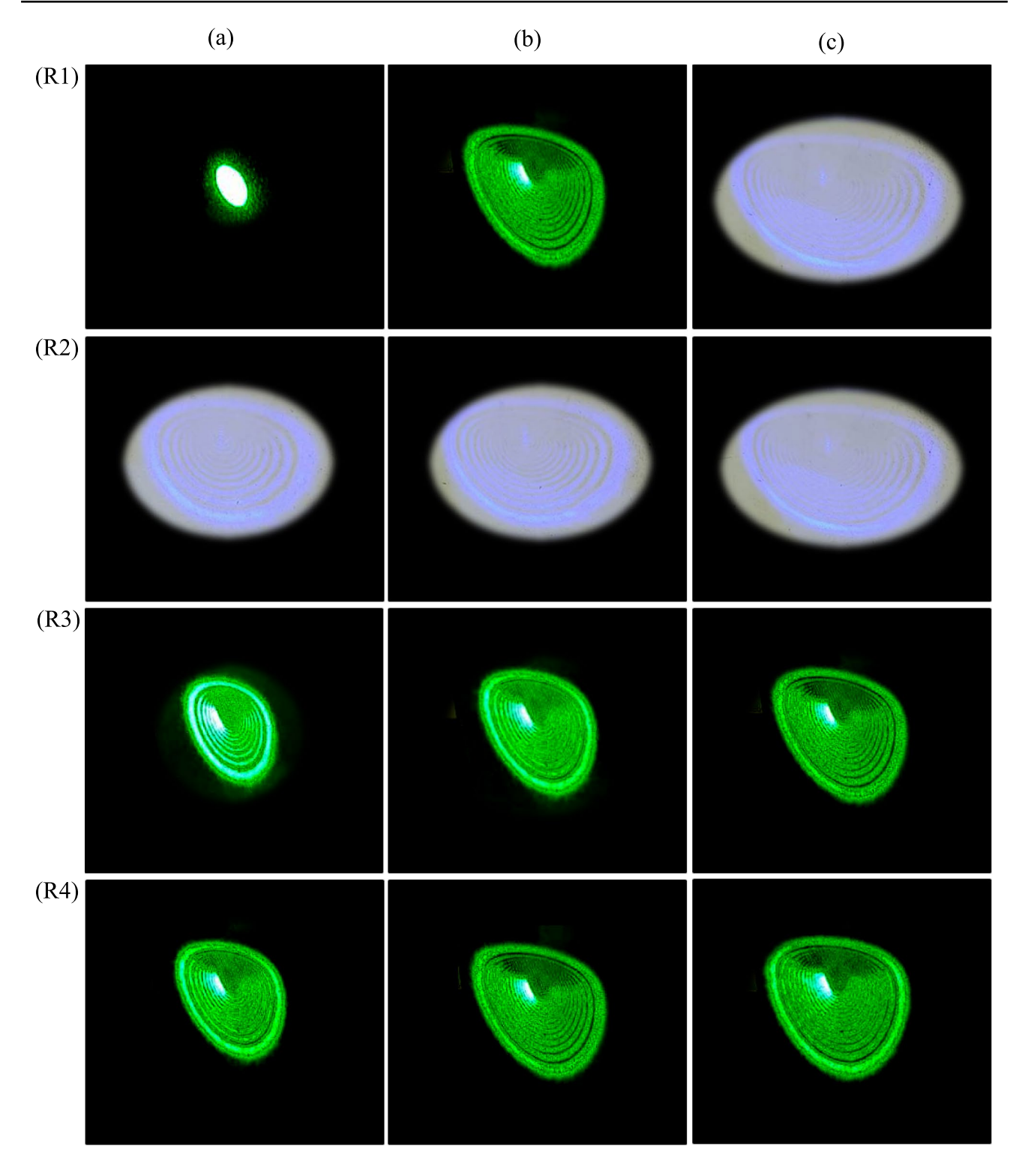


Fig. 17 Static AOS in the azo compound

71 Page 14 of 27 M. J. Ashoor et al.

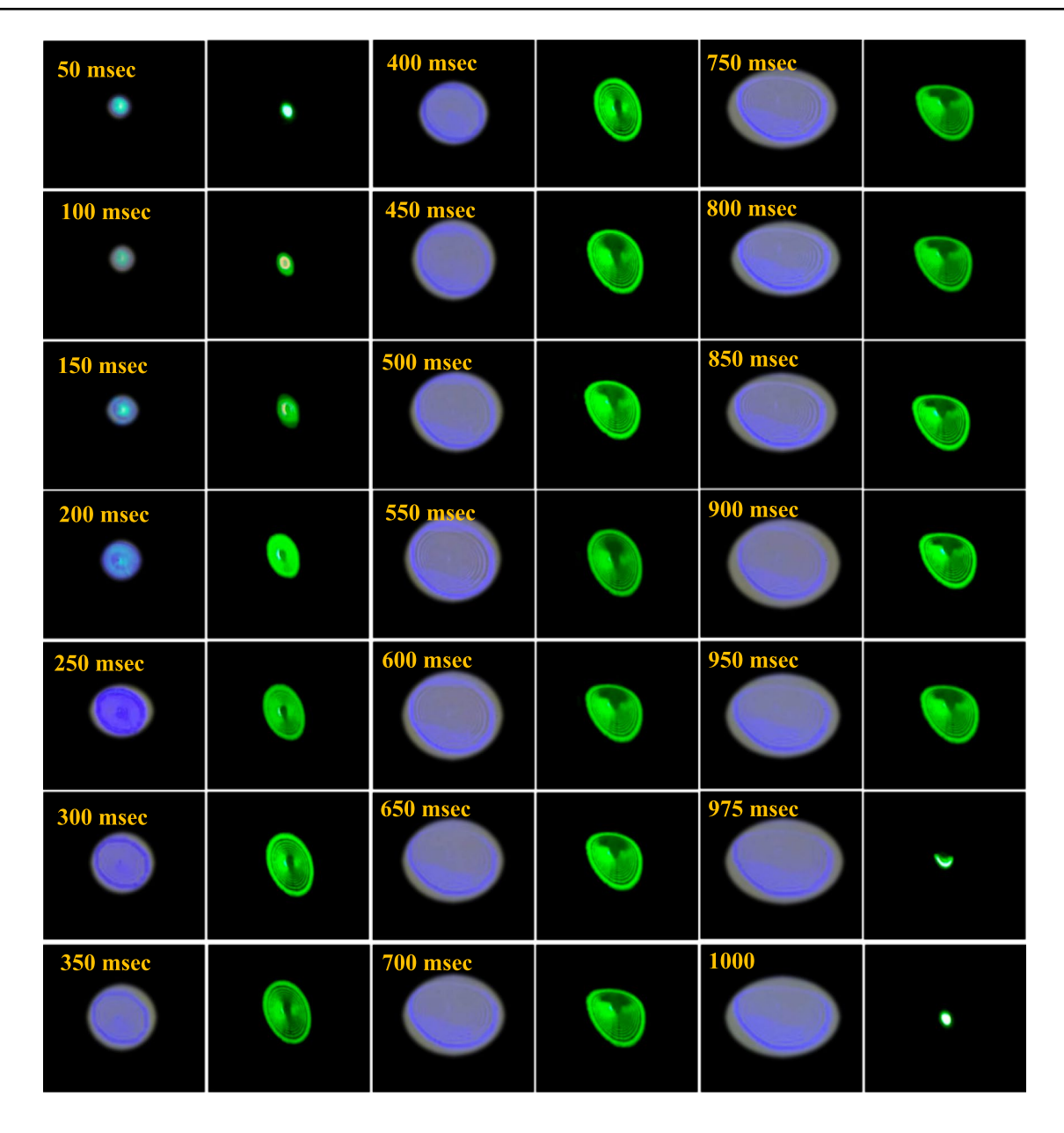


Fig. 18 Dynamic AOS in the azo compound

$$E_{o}(x,y,t,z=0) = \left(\frac{2P}{\pi\omega^{2}}\right)^{1/2} exp\left(-\frac{x^{2}+y^{2}}{\omega^{2}}\right) \cdot exp\left[-i\left(k\frac{x^{2}+y^{2}}{2R}\right)\right] \endaligned (3)$$

As the medium heat increased two types of thermal currents developed: conduction one horizontally and convection one vertically. When both currents are equal, the resulted DPs usually appeared symmetrically distributed in the x-y plane. When the vertical thermal current exceeds the horizontal thermal current, the DPs appeared compressed, i.e., the DPs appear asymmetric. Such behavior has been seen to occur in this work (see Sect. 3.4). Post the beam propagation

through the nonlinear medium, the beam complex amplitude can be written as follows [78]:

$$\begin{split} E(x, y, zt, z &= 0) \\ &= \left(\frac{2P}{\pi\omega^2}\right)^{1/2} exp\left(-\frac{\alpha d}{2}\right) exp\left(-\frac{x^2 + y^2}{\omega^2}\right) \\ &\cdot exp\left[-i\left(k\frac{x^2 + y^2}{2R}\right) exp(\Delta\phi(x, y, t))\right] \end{split} \tag{4}$$



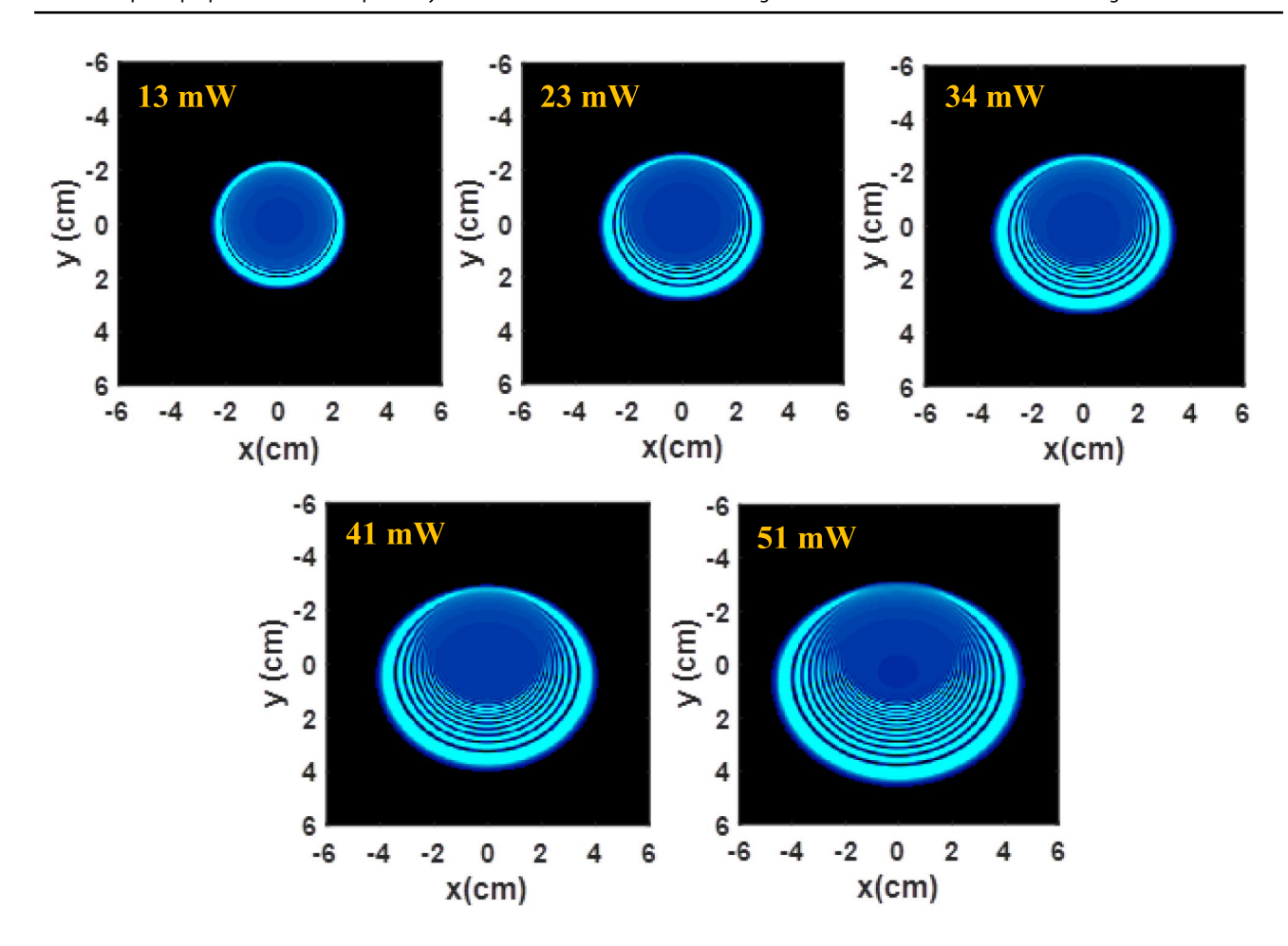


Fig. 19 Numerical estimation of power input on the type of DPs in the azo compound

d is the sample thickness. Based on the Fraunhofer approximation and using Fresnel-Kirchhoff integral, the complex amplitude of the laser beam in the far field a distance D from the exit plane of the sample cell is written as follows [78]:

$$\begin{split} &E\left(x',y,t'\right) \\ &= \left(\frac{2P}{\pi\omega^2}\right)^{1/2} \frac{i\pi\omega^2}{\lambda D} \exp\left(ikD\right) \exp\left(-\frac{\alpha d}{2}\right) \int\limits_{-\infty}^{\infty} dx \int\limits_{-\infty}^{\infty} dy \exp\left(-\frac{x^2+y^2}{\omega^2}\right) \\ &\cdot \exp\left[-i\left(k\frac{x^2+y^2}{2R} + \Delta\phi(x,y,t)\right)\right] \exp\left[-ik\left(\frac{xx'+yy'}{D}\right)\right] \end{split} \tag{5}$$

and the light intensity on the screen is written as follows [78]:

$$\begin{split} &I\left(x',y',t'\right) \\ &= \left| \left(\frac{2P}{\pi\omega^2}\right)^{1/2} \frac{i\pi\omega^2}{\lambda D} \exp\left(ikD\right) \exp\left(-\frac{\alpha d}{2}\right) \int\limits_{-\infty}^{\infty} dx \int\limits_{-\infty}^{\infty} dy \exp\left(-\frac{x^2+y^2}{\omega^2}\right) \right. \\ &\left. \cdot \exp\left[-i\left(k\frac{x^2+y^2}{2R} + \Delta\phi(x,y,t)\right)\right] \exp\left[-ik\left(\frac{xx'+yy'}{D}\right)\right]\right|^2 \end{split} \tag{6}$$

x' and y' are the spatial coordinates on the screen.

Equation (6) is solved numerically using MATLAB system.

Figures 19, 20 and 21 shows the simulation results of the effect of power input, wave front, and the temporal evolution of the DPs. Figures 22, 23 and 24 are the simulation results of the two-dimensional variation of the beam phase (left column) and the one-dimensional x-axis (middle column). and the one-dimensional y-axis (right column) of the light intensity against the variation of power input and beam wavefront and temporal variations of DPs. Figures 25, 26 and 27 are the estimation results of the two-dimensional variation of the medium temperature (left column) and the one-dimensional x-axis (middle column) and the one-dimensional y-axis (right column) of the light intensity against the variation of power input and beam wave front and temporal variations of DPs.



71 Page 16 of 27 M. J. Ashoor et al.

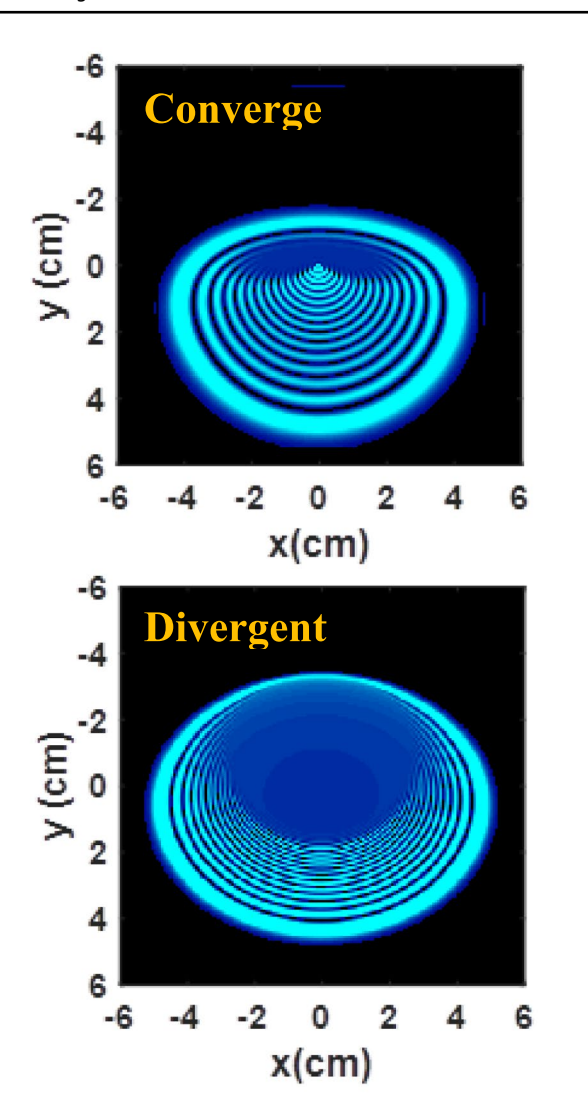


Fig. 20 Numerical estimation of the wavefront type of DPs in the azo compound

3.6 Determine the NLRI, n2, due to

3.6.1 DPs

Based on the work of Durbin et al. [79] and Ogusu et al. [80], the NLRI, n_2 , of azo compound can be estimated using the following equation [80]

$$n_2 = \frac{\Delta n}{I} \tag{7}$$

 Δn is the change of the azo compound refraction index and I is the high beam intensity that can be written as follows:



 P_{max} is the maximum input power of the laser beam and ω is the laser beam sport size at the entrance of the sample cell at e^{-2} . Δn can be obtained using the following equation

$$\Delta n = \frac{N\lambda}{d} \tag{9}$$

N is the number of rings at P_{max} , is the beam wavelength and d is the sample cell thickness. For N=10, $\omega=19.235$ μm , $P_{max}=51$ mW, $\lambda=473$ nm, d=1 mm, so that Δn and n_2 are 4.73×10^{-3} and 5.38×10^{-7} cm²/W for the azo compound.

3.6.2 Z-scan

Based on the Sheik Bahae [35, 36], the NLAC, β , and NLRI, n_2 , can be determine by the following equation [36]

$$\beta = \frac{2\sqrt{2}\Delta T}{L_{\text{eff}}I} \tag{10}$$

$$n_2 = \frac{\Delta \phi \lambda}{2\pi L_{\text{eff}} I} \tag{11}$$

$$\Delta T = 1 - T_{\rm p} \tag{12}$$

$$L_{\text{eff}} = \frac{1 - \exp\left(-\alpha d\right)}{\alpha} \tag{13}$$

$$\Delta \varphi_o = \frac{\Delta T_{p-v}}{0.406(1-S)^{0.25}} \tag{14}$$

$$\Delta T_{p-v} = T_p - T_v \tag{15}$$

$$L_{\text{eff}} = \frac{1 - \exp\left(-\alpha d\right)}{\alpha} \tag{16}$$

 $L_{\rm eff}$ is sample effective thickness, $T_{\rm v}$ and $T_{\rm p}$ are the valley and peak transmittances, $\Delta \varphi_o$ is the on-axis phase shift, and S is linear transmittance of aperture. The value of NLAC, β , and NLRI, n_2 , of the azo compound can calculated using Eqs. 10–16, and found to be 2.03×10^{-3} cm/W and 3.16×10^{-7} cm²/W respectively for the azo compound. The NLRI obtained from the present azo compound can be well compared to those obtained for compounds studied in Refs. [81–90] where it can be seen that the azo compound's value is higher or of the same order so that it can be used in photonic applications.



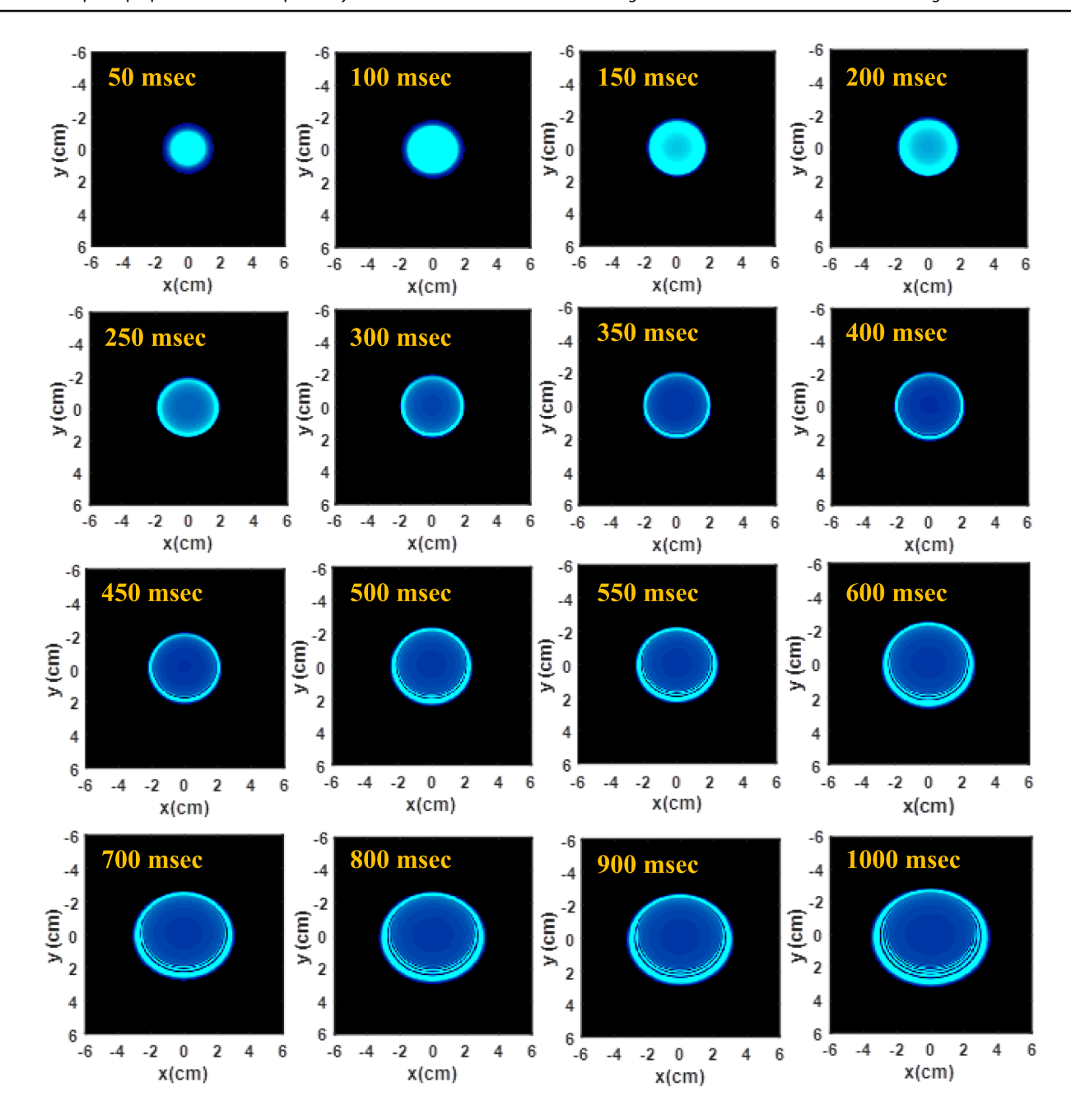


Fig. 21 Numerical estimation of the temporal evolution of a chosen DP in the azo compound

4 Conclusion

The compound (E)-4-((3-(tert-butyl)-2-hydroxy-5-methoxyphenyl) diazenyl) is synthesized via diazonation of sulfadiazine. The azo compound, or -N-(pyrimidin-2-yl) benzenesulfonamide, is produced when sulfadiazine dissolves in a diluted hydrochloric acid solution and goes through a diazonation reaction. The azo molecule was further analyzed using mass spectrometry, FTIR, and ¹H and ¹³C NMR spectra. The nonlinear refractive index (NLRI)

and the nonlinear absorption coefficient (NLAC) were measured using two approaches, namely the Z-scan and diffraction patterns (DPs), under irradiation with a continuous wave laser beam with a wavelength of 473 nm. We have shown that the DPs are contingent upon the characteristics of the beam wavefront, the amount of power supplied, and the duration of time. The distortion of the resulted DPs in the upper half is related to the vertical convection thermal currents. The convection is due to the collapsed laser beam.



71 Page 18 of 27 M. J. Ashoor et al.

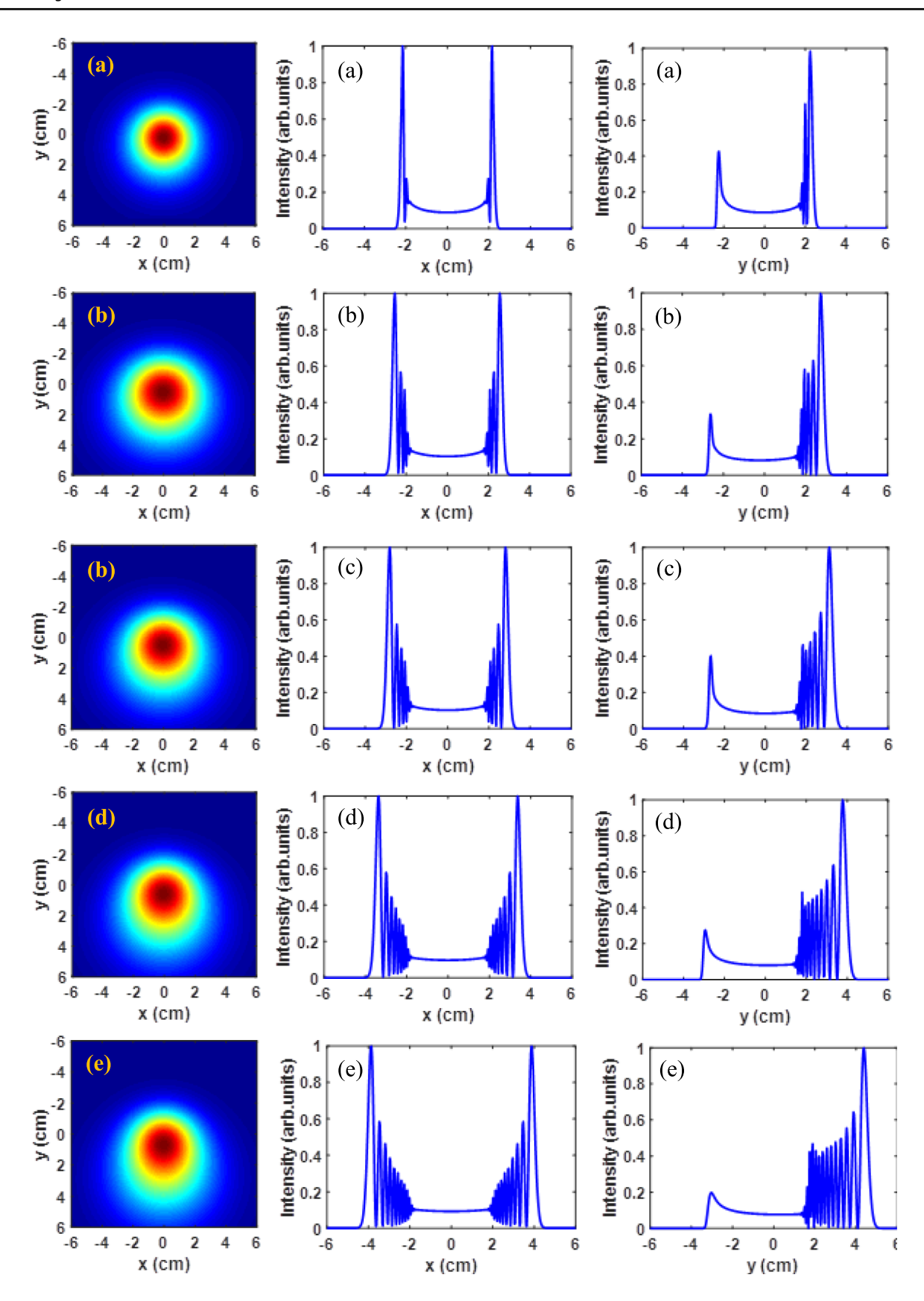


Fig. 22 Numerical estimation of (left column) beam phase two-dimensional variations, (middle column) intensity variations along the x-axis, (right column) intensity variation along y-axis in the azo compound



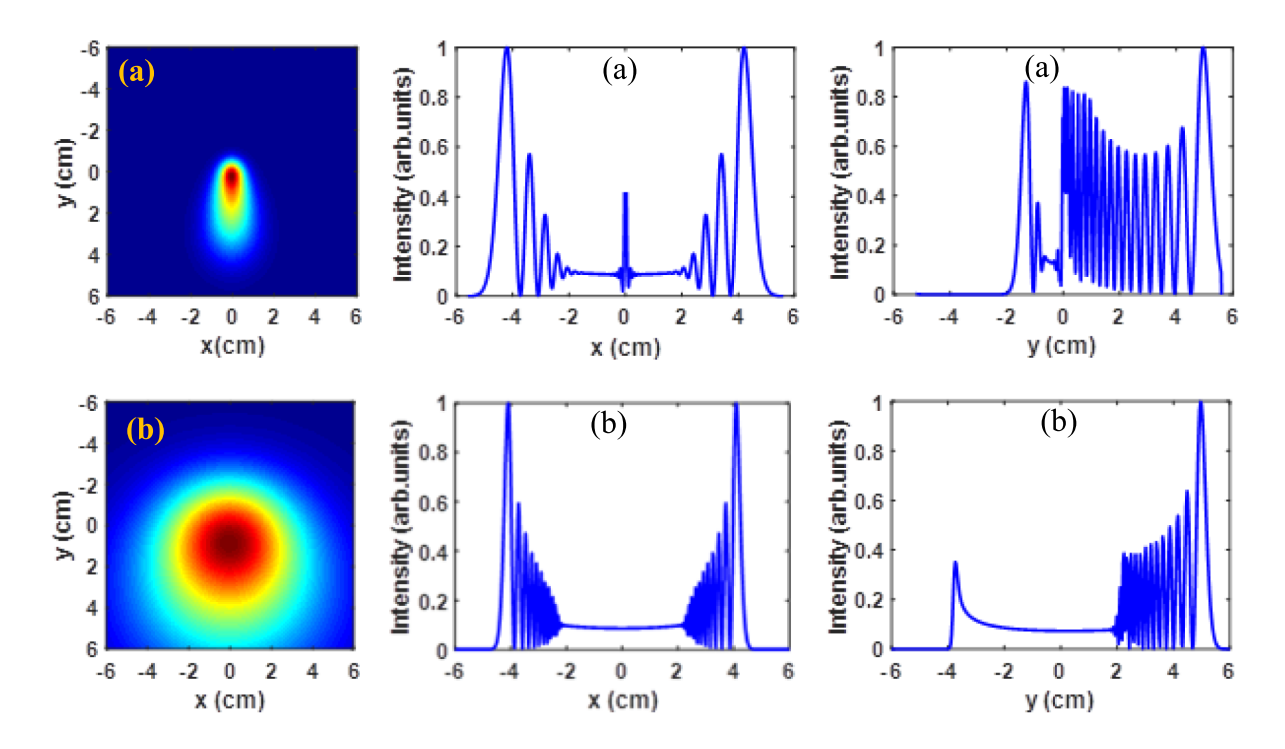


Fig. 23 Same as Fig. 22 against beam wave front in the azo compound

Diffractive optics were employed to attain non-linear refractive index (NLRI) values as high as 5.38×10^{-7} cm²/W and 3.16×10^{-7} cm²/W due to the Z-scan. The Z-scan technique was also utilized to obtain nonlinear absorption coefficient (NLAC) values of 2.03×10^{-3} cm/W. The DPs were quantitatively and qualitatively analyzed using the Fresnel-Kirchhoff

integral. The azo compound utilizes a process called alloptical switching, which involves the use of two laser beams with wavelengths of 473 nm and 532 nm. The purpose of the present work is achieved through the synthesis of a new azo compound with high nonlinear optical properties.



71 Page 20 of 27 M. J. Ashoor et al.

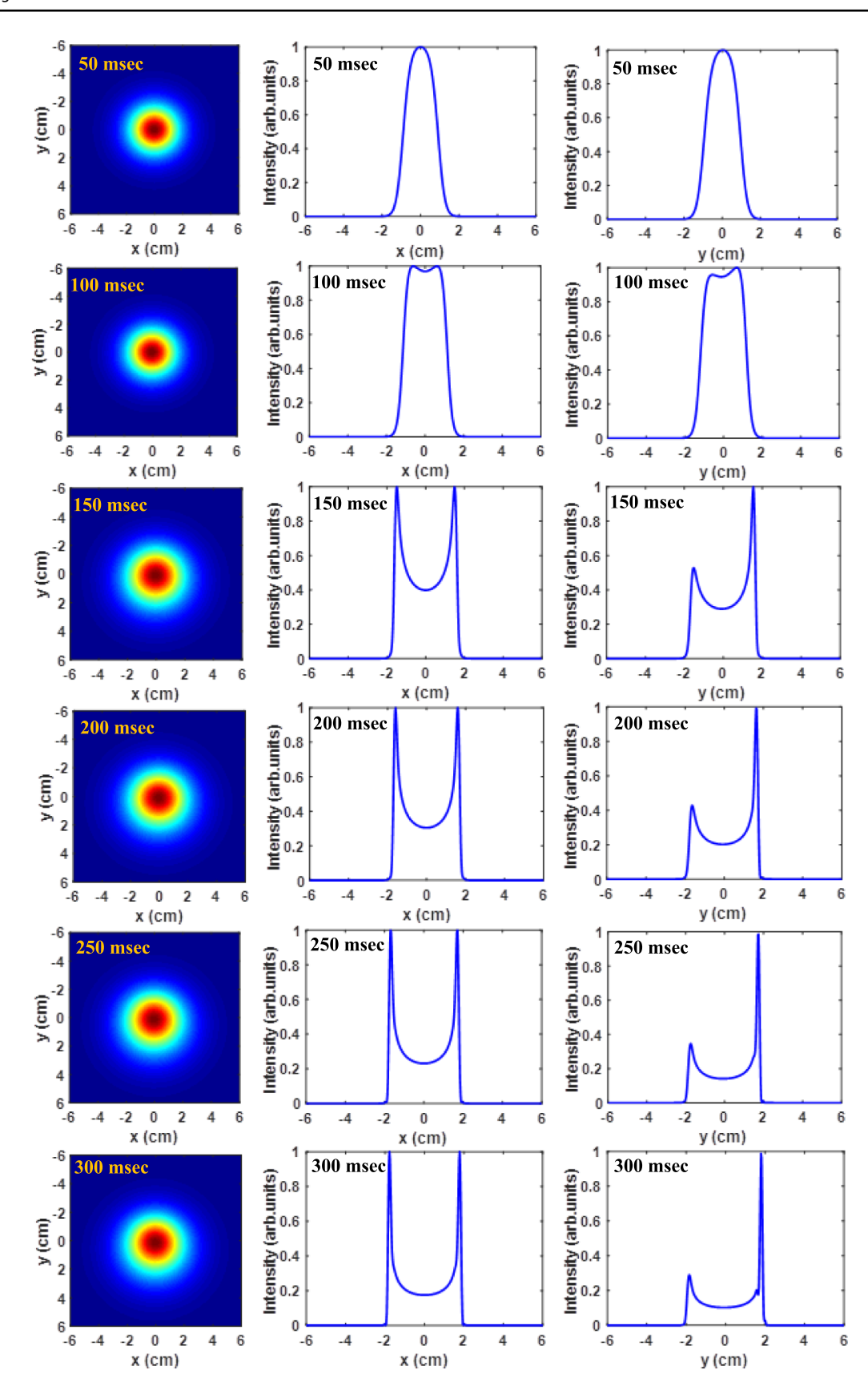


Fig. 24 Same as Fig. 22 for temporal evolution in the azo compound



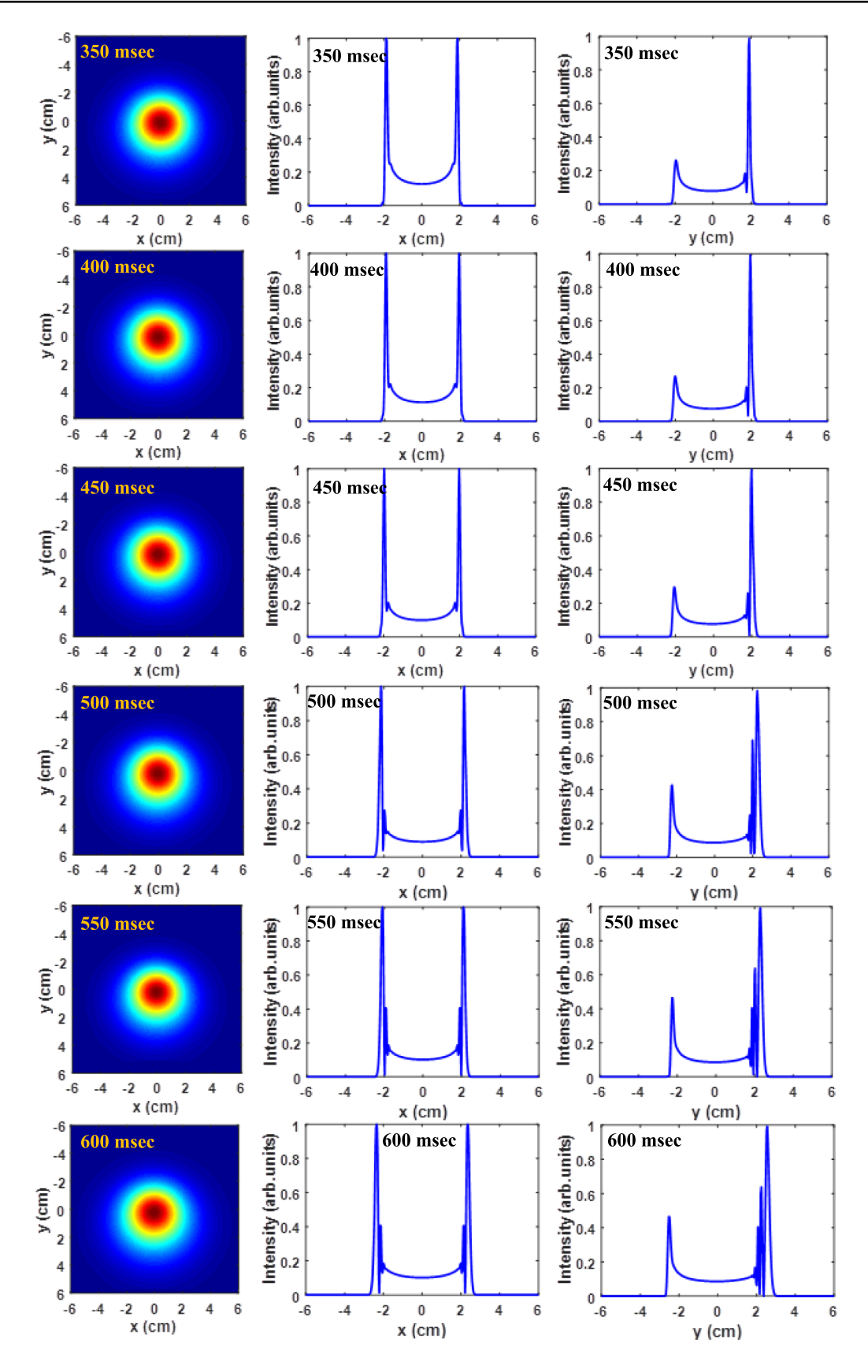
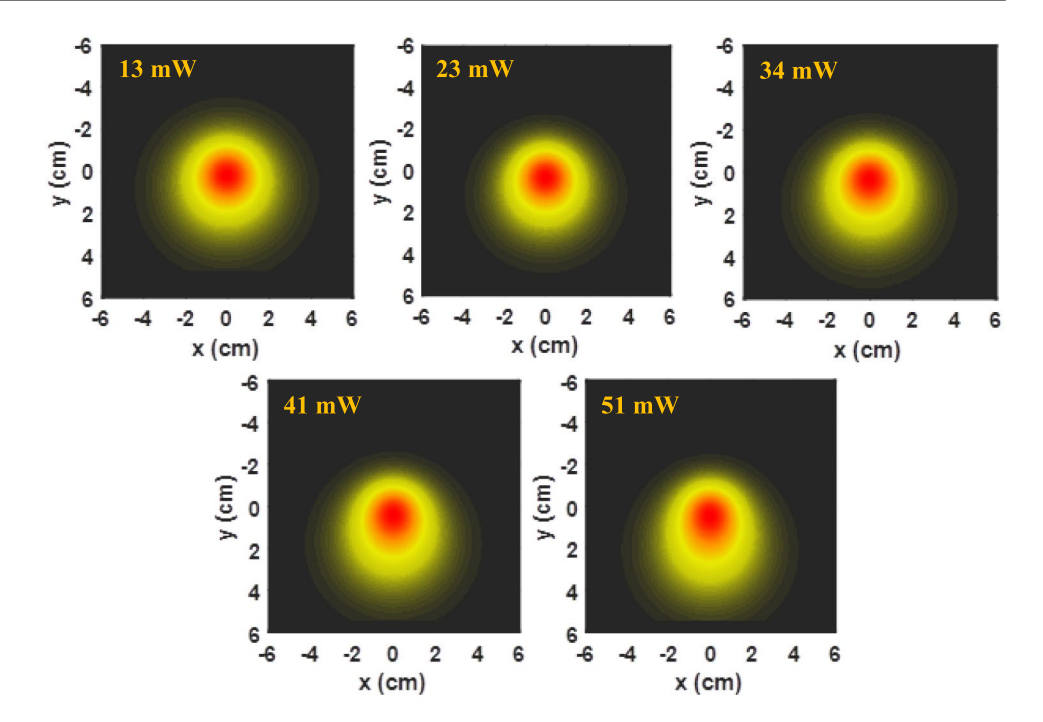


Fig. 24 (continued)



Fig. 25 Same as Fig. 19 for the two-dimensional temperature variation in azo compound





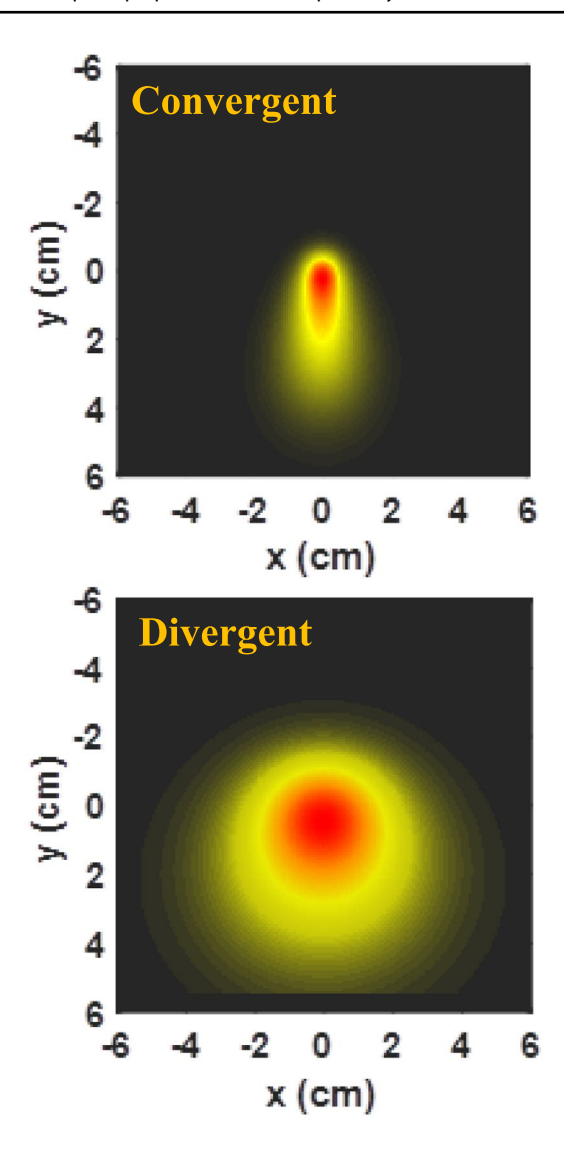


Fig. 26 Same as Fig. 20 for the two-dimensional temperature variation in the azo compound



71 Page 24 of 27 M. J. Ashoor et al.

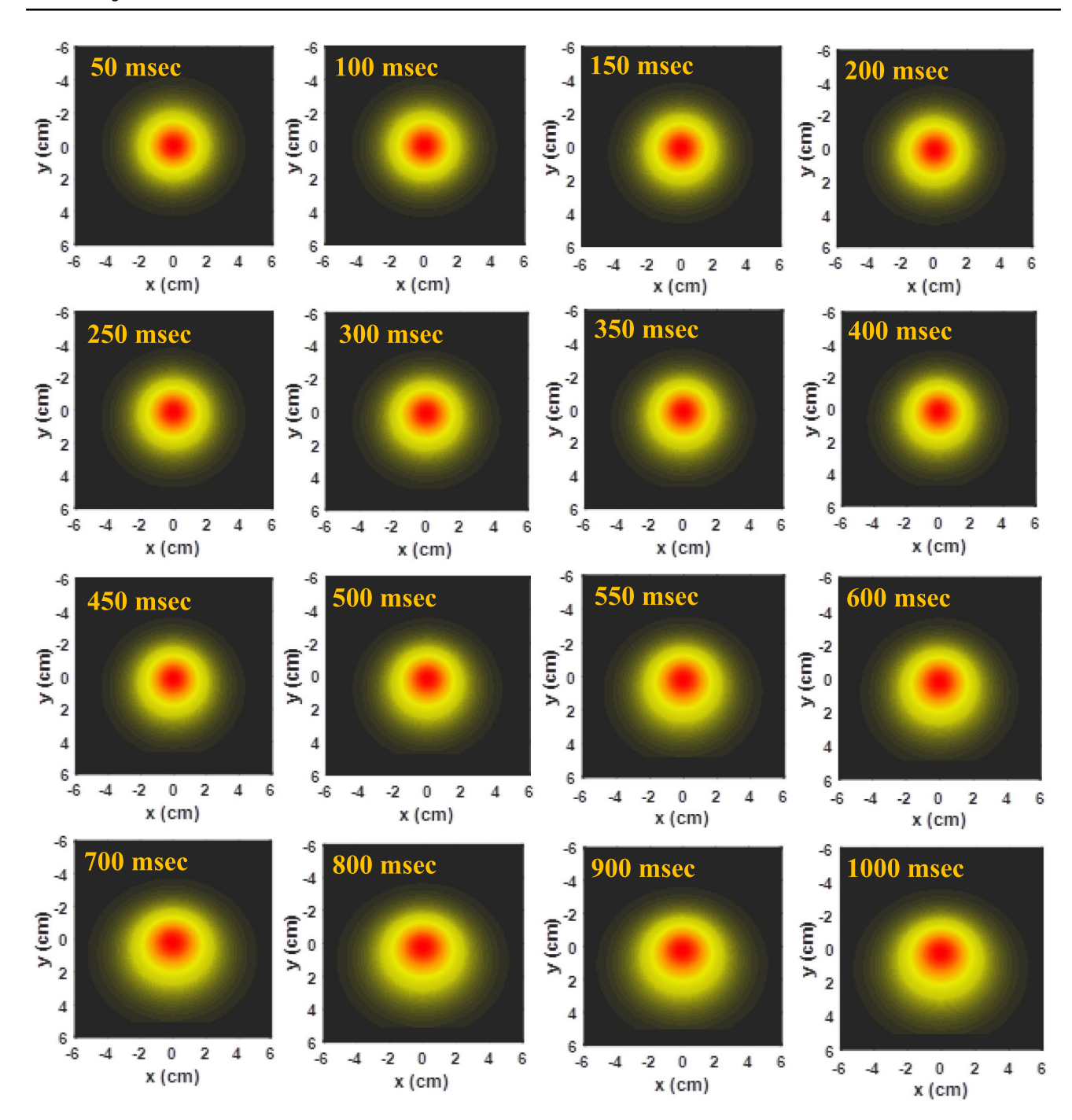


Fig. 27 Same as Fig. 21 the two-dimensional temperature variation in the azo compound



Author contributions M. J. Ashoor taking measurements, Sadiq M. H Ismael synthesis the compound, Hanadi M. Jarallah and H. A. Sultan participated in the characterization and analysis of the results, Qusay M.A. Hassan and Kawkab Ali Hussein wrote the main manuscript, C. A. Emshary wrote the main manuscript text—review & editing. All authors reviewed the manuscript.

Data availability No datasets were generated or analysed during the current study.

Declarations

Conflict of interest The authors declare no competing interests.

References

- Kh.A. Al-Timimy, H.A. Sultan, Q.M.A. Hassan, C.A. Emshary, A.Q. Abdullah, E.A.R. Arebi, The preparation and nonlinear properties study of a mixture of polyurethane and neutral red dye solution. J. Fluoresc. 33, 1761–1776 (2023)
- M.D. Zidan, A.W. Allaf, Z. Ajji, A. Allahham, Optical limiting behavior of Sudan III dye doped polymer. Opt. Laser Technnol. 42, 531–533 (2010)
- H.M. Ozaktas, M.A. Kutay, Optical information processing: A historical overview. Digit. Signal Process. 119, 103248 (2021)
- K. Seevakan, P. Myrizhi, Nonlinear optics material harmonic generation. Int. J. Pure Appl. Math. 119, 5651–5660 (2018)
- 5. A.R. Pandem, S.M. Gulhane, Optical computing. Int. J. Adv. Electr. Electron. Eng. 2, 147–150 (2013)
- I. Luc, J. Niziol, M. Sniechowski, B. Sahraoui, J.-L. Fillano, O. Krupka, Study of nonlinear optical and structure properties of orgomometallic complexes. Mol. Cryst. Liq. Cryst. 485, 1–13 (2008)
- W. Blau, Organic materials for nonlinear optical devices. Phys. Technol. 18, 250–268 (1987)
- R.S. Potember, R.C. Hoffman, K.A. Stetyick, R.A. Murphy, K.R. Speck, Molecular materials for nonlinear optics. Johns Hopkins APL Technol. Dig. 9, 189–199 (1988)
- F. Limosani, F. Tessore, G. Oi Carlo, A. Fomi, P. Tagliatesta, Nonlinear optical properties of prohyrin, fullererne and ferrocene hybrid materials. Materials 14, 4404 (2021)
- A.M. Jassem, Q.M.A. Hassan, C.A. Emshary, H.A. Sultan, F.A. Almashal, W.A. Radhi, Synthesis and optical nonlinear properties performance of azonaphthol dye. Phys. Scr. 96, 025503 (2021)
- Q.M.A. Hassan, H.A. Sultan, A.S. Al-Asadi, A.J. Kadhim, N.A. Hussein, C.A. Emshary, Synthesis, characterization, and study of the nonlinear optical properties of two new organic compounds. Synth. Met. 257, 116158 (2019)
- Q.M.A. Hassan, N.A. Raheem, C.A. Emshary, A.M. Dhumad, H.A. Sultan, T. Fahad, Preparation, DFT and optical nonlinear studies of a novel azo-(β)- diketone dye. Opt. Las. Technol. 148, 107705 (2022)
- A.M. Dhumad, Q.M.A. Hassan, C.A. Emshary, T. Fahad, N.A. Raheem, H.A. Sultan, Nonlinear optical properties investigation of a newly synthesised Azo-(β)- diketone dye. J. Photochem. Photobiol. A Chem. 418, 113429 (2021)
- A.M. Jassem, Q.M.A. Hassan, F.A. Almashal, H.A. Sultan, A.M. Dhumad, C.A. Emshary, L.T.T. Albaaj, Spectroscopic study, theoretical calculations, and optical nonlinear properties of amino acid (glycine)-4-nitro benzaldeyhyde-derived Schiff base. Opt. Mater. 122, 111750 (2021)

- C.A. Emshary, Q.M.A. Hassan, H. Bakr, H.A. Sultan, Determination of the optical constants, nonlinear optical parameters and threshold limiting of methyl red-epoxy resin film. Physica B 622, 413354 (2021)
- C.A. Emshary, I.M. Ali, Q.M.A. Hassan, H.A. Sultan, Linear and nonlinear optical properties of potassium dichromate in solution and solid polymer film. Physica B 613, 413014 (2021)
- S.K. Khalaf, Q.M.A. Hassan, C.A. Emshary, H.A. Sultan, Concentration effect on optical properties and optical limiting of PVA doped with nigrosin films. J. Photochem. Photobiol. A Chem. 427, 113809 (2022)
- A.H. Ali, H.A. Sultan, Q.M.A. Hassan, C.A. Emshary, Thermal and nonlinear optical properties of sudan III. J. Fluoresc. 34, 635–653 (2024)
- Q.M.A. Hassan, C.A. Emshary, H.A. Sultan, Investigating the optical nonlinear properties and limiting optical of eosin methylene blue solution using a cw laser beam. Phys. Scr. 96, 095503 (2021)
- J.K. Salim, Q.M.A. Hassan, A.M. Jassem, H.A. Sultan, A.M. Dhumad, C.A. Emshary, An efficient ultrasound-assisted CH3COONa catalyzed synthesis of thiazolidinone molecule: Theoretical and nonlinear optical evaluations of thiazolidinone-Schiff base derivative. Opt. Mater. 133, 112917 (2022)
- S.A. Ali, Q.M.A. Hassan, C.A. Emshary, H.A. Sultan, Characterizing optical and morphological properties of Eriochrome Black T doped polyvinyl alcohol film. Phys. Scr. 95, 095814 (2020)
- Q.M.A. Hassan, H. Bakr, C.A. Emshary, H.A. Sultan, Studying the surface morphology, optical and nonlinear optical properties of epoxy resin doped nickel nitrate film. Optik 213, 164771 (2020)
- G. Wang, F. Gar, Optical parameters, and absorption studies of azo-dye-doped polymer thin films on silicon. Mater. Lett. 43, 6–10 (2000)
- W. Bin, W. Yi-Qun, G. Dong-Hong, G. Fu-Xi, optical parameters and absorption of azo dye ant it's metal-substituted compound thin films. Chin. Phys. Lett. 20, 1596–1599 (2003)
- P.D.S. Roslan, S. Senthil, P. Kaunan, G. Vinicha, A. Ramalingam, Investigation on substituent effect in novel azo-naphthol dyes containing polymethacrylates for nonlinear optical studies. J. Phys. Chem. 68, 1812–1820 (2007)
- O.G. Morales-Saavedra, T. Garcia, C. Caicedo, E. Rivera, Nonlinear optical properties of new amphiphilic azo polymer bearing well defined oligo (ethylene glycol) spacers. Rev. Mex. DE Fis. 56, 449–455 (2010)
- S. Aithal, P.S. Aithal, G.K. Phat, comparative study on azo-dyedoped polymer films for optical phase conjugation. Int. J. Sci. Res. 4, 436–441 (2013)
- M. Parvin, B. Ahmed, Investigation of optical limiting properties of azophoxine dye using nanosecond z-scan technique. Int. J. Chem. Tech. Res. 6, 2493–2498 (2014)
- E. Ouskova, A. Pshenychni, A. Sanchez-Ferrer, B. Lysenko, J. Vapravuori, M. Kaivola, Enhanced nonlinearing by H-bonded polymer-dope complex in liquid crystal for holographic gratings. J. Opt. Soc. Am. B 31, 1456–1464 (2014)
- M.F. Al-Mudhaffer, A.Y. Al-Ahmad, Q.M.A. Hassan, C.A. Emshary, Optical characterization and all-optical switching of bezenesulfonanide azo-dye. Optik 127, 1160–1166 (2016)
- S. Sharifi, G.L. Faritovna, A. Azarpour, Photophysical and nonlinear optical properties of azophloxine in reverse micelles. J. Fluoresc. 28, 1439–1450 (2018)
- A.D. Vargas-Varga, E. Vargas, F.R. Castellanos-Duran, J. Mejoradu, M.A. Isidro-Ojeda, E. Cedeno-Berani, J.B. Rojas-Trigos, A.G. Juarez, G.A. Calderon, E. Marin, Thermal lens spectroscopy. Lat. Am. J. Phys. Educ. 16, 3313 (2022)



71 Page 26 of 27 M. J. Ashoor et al.

- J.P. Gordon, R.C. Leite, R.S. Moore, S.P.S. Porto, J.R. Whinner, Long-transient effect: in lasers with inserted liquid samples. J. Appl. Phys. 36, 3–8 (1965)
- W.R. Callen, B.G. Huth, R.H. Pantell, Optical patterns of thermally self-defocused light. Appl. Phys. Lett. 11, 103–105 (1967)
- 35. M. Sheik-Bahae, A.A. Said, E.W. Van Stryland, High sensitivity single beam n₂ measurements. Opt. Lett. **14**, 955–957 (1989)
- M. Sheik-Bahae, A.A. Said, T. Wei, D.J. Hagan, E.W. Van Stryland, Sensitive measurement of optical nonlinearities using a single beam. IEEE J. Quantum Electron. QE 26, 760–769 (1990)
- S. Benkhaya, S. M'rabet, A. El Harfi, Classifications, properties, recent synthesis, and applications of azo dyes. Heliyon 6, e03271 (2020)
- F. Eltaboni, N. Bader, R. El-Kailany, N. Elsharif, A. Ahmida, Original article: chemistry and applications of azo dyes: a comprehensive review. J. Chem. Rev. 4, 313–330 (2022)
- M. Di Martino, L. Sessa, M. Di Matteo, B. Panunzi, S. Piotto, S. Concilio, Azobenzene as antimicrobial molecules. Molecules 27, 5643 (2022)
- N.M. Mallikarjuna, J. Keshavayya, Synthesis, spectroscopic characterization and pharmacological studies on novel sulfamethaxazole based azo dyes. J. King Saud Univ. Sci. 32, 251–259 (2020)
- A.R. Sayed, H. Elsawy, S. Shaaban, S.M. Gomha, Y.S. Al-Faiyz, Design, synthesis, and biological evaluations of novel azothiazoles based on thioamide. Curr. Issues Mol. Biol. 44, 2956–2966 (2022)
- C. Luoa, O. Borodinb, X. Ji, S. Houa, K.J. Gaskelld, X. Fana, J. Chena, T. Denga, R. Wangd, J. Jiangc, C. Wanga, PNAS 115, 2004–2009 (2018)
- G. Ziyatdinova, M. Titova, R. Davletshin, Electropolymerized 4-aminobenzoic acid based voltammetric sensor for the simultaneous determination of food Azo dyes. Polymers 14, 5429 (2022)
- A. Chevalier, P.-Y. Renard, A. Romieu, Azo-based fluorogenic probes for biosensing and bioimaging: recent advances and upcoming challenges. Chem. Asian J. 12, 2008–2028 (2017)
- Z. Essaidi, J. Niziol, B. Sahraoui, Azo-azulene based compoundsnonlinear optical and photorefractive properties. Opt. Mater. 33, 1387–1390 (2011)
- D.A. Hassan, H.A. Sultan, R.H. Al-Asadi, Q.M.A. Hassan, C.A. Emshary, T. Fahad, DFT calculation and nonlinear optical properties of (E)-(2)-((8-hydroxyquinolin-5yl)diazenyl)-5-sulfamoylpheneyl)mercury(II) chloride. Phys. B Condens. Matter 639, 413908 (2022)
- D. Chomicki, O. Kharchenko, L. Skowronski, J. Kowalonek, A. Kozanecka-Szmigiel, D. Szmigiel, V. Smokal, O. Krupka, B. Derkowska-Zielinska, Int. J. Mol. Sci. 21, 5755 (2020)
- U.J. Al-Hamdani, Q.M.A. Hassan, A.M. Zaidan, H.A. Sultan, K.A. Hussain, C.A. Emshary, Z.T.Y. Alabdullah, J. Mol. Liq. 361, 119676 (2022)
- K.I. Ramachandran, G. Deepa, K. Namboori, Computational Chemistry and Molecular Modeling Principles and Applications (Springer, 2008). https://doi.org/10.1007/978-3-540-77304-7
- D.L. Pavia, G.M. Lampman, G.S. Kriz, Introduction to Spectroscopy A Guide for Students of Organic Chemistry (Thomson Learning Academic Resource Center, USA, 2001)
- Y. Jia, Y. Shan, L. Wu, X. Dai, D. Fan, Y. Xiang, Broadband nonlinear optical resonance, and all-optical switching of liquid phase exfoliated tungsten diselenide. Photonics Res. 5, 1040–1047 (2018)
- Q. Wang, X. Wu, L. Wu, Y. Xiang, Broadband nonlinear optical response in Bi2Se2-Bi2Te3 heterostructure and its application in all-optical switching. AIP Adv. 9, 025022 (2019)
- X.J. Zhang, Z.H. Yuan, R.X. Yang, Y. He, Y.L. Qin, X. Si, H. Jun, A review on spatial self-phase modulation of two-dimensional material. J. Cent. South Univ. 26, 2295–2306 (2019)

- S. Jeyaram, Intermolecular charge transfer in donor–acceptor substituted triarylmethane dye for NLO and optical limiting applications. J. Mater. Sci. Mater. Electron. 32, 9368–9376 (2021)
- E. Neil, Jacobsen, NMR data interpretation explained understanding 1D and 2D NMR spectra of organic compounds and natural products (Wiley, Hoboken, 2017)
- M.J. Frisch et al., Gaussian 09, Revision E.01 (Gaussian Inc., Wallingford CT, 2009)
- U.J. Al-Hamdani, Q.M.A. Hassan, C.A. Emshary, H.A. Sultan, A.M. Dhumad, A.A. Al-Jaber, All optical switching and the optical nonlinear properties of 4-(benzothiazolyldiazenyl)-3-chlorophenyl 4-(nonylthio)benzoate (EB-3Cl). Optik 248, 168196 (2021)
- Q.M.A. Hassan, R.H. Al-Asadi, H.A. Sultan, H.A. Abdullmajed, S.A. Ali, C.A. Emshary, A novel azo compound derived from ethyl-4-amino benzoate: synthesis, nonlinear optical properties and DFT investigations. Opt. Quantum Electron. 55, 392 (2023)
- H. Louis, O.C. Enudi, J.O. Odey, I.B. Onyebuenyi, A.T. Igbalagh, T.O. Unimuke, T.N. Ntui, Synthesis, characterization, DFT, and TD-DFT studies of (E)-5-((4,6-dichloro-1,3,5-tria-zin-2-yl) amino)-4 -hydroxy-3-(phenyldiazenyl) naphthalene-2,7-diylbis(hydrogen sulfte). SN Appl. Sci. 3, 712 (2021)
- J. Zhao, Y. Zhang, L. Gan, G. Wang, Experimental and DFT study of UV-vis absorption spectra of azobenzene containing ester groups. Comput. Theor. Chem. 1200, 113244 (2021)
- N. Singh, M. Arish, P. Kumar, A. Rub, U. Riaz, Experimental and theoretical studies of novel azo benzene functionalized conjugated polymers: In-vitro antileishmanial activity and bioimaging. Sci. Rep. 10, 57 (2020)
- A. Abu El-Fadl, G.A. Mohamad, A.B. Abd El-Moiz, M. Rashad, Optical constants of Zn_{1-x}Li_x O films prepared by chemical bath decomposition technique. Physica B 366, 44–54 (2005)
- H. Shokry, E.M. Mabrouk, Computational and electrochemical investigation for corrosion inhibition of nickel in molar sulfuric acid by dihydrazide derivatives. Part II. Arab. J. Chem. 10, S3402–S3411 (2017)
- 64. M. Miar, A. Shiroudi, K. Pourshamsian, A.R. Oliaey, F. Hatam-jafari, Theoretical investigations on the HOMO–LUMO gap and global reactivity descriptor studies, natural bond orbital, and nucleus-independent chemical shifts analyses of 3-phenylbenzo[d] thiazole-2(3H)-imine and its para-substituted derivatives: Solvent and substituent effects. J. Chem. Res. 45, 147–158 (2021)
- S.F. Nelsen, M.N. Weaver, A.E. Konradsson, J.P. Telo, T. Clark, Electron transfer within 2,7-dinitronaphthalene radical anion. J. Am. Chem. Soc. 126, 15431–15438 (2004)
- 66. L.H. Abdel-Rahman, A.M. Abu-Dief, H. Moustafa, A.A.H. Abdel-Mawgoud, Design and nonlinear optical properties (NLO) using DFT approach of new Cr(III), VO(II), and Ni(II) chelates incorporating Tri-dentate imine ligand for DNA interaction, antimicrobial, anticancer activities and molecular docking studies. Arab. J. Chem. 13, 649–670 (2020)
- N. Senthilvelan, G. Rajarajan, A. Jegatheesan, S. Sivakumar, Growth and spectroscopic characterization of urea sulphamic acid crystal: a second -order nonlinear material. Rasayan J. Chem. 10, 218–225 (2017)
- S. Bullo, R. Jawaria, I. Faiz, I. Shafiq, M. Khalid, M.A. Asghar, R. Baby, R. Orfali, S. Perveen, Efficient synthesis, spectroscopic characterization, and nonlinear optical properties of novel salicylaldehyde-based thiosemicarbazones: experimental and theoretical studies. ACS Omega 8, 13982–13992 (2023)
- S.F. Lópeza, M.P. Mezaa, F.T. Hoyos, Study of the nonlinear optical properties of 4-nitroaniline type compounds by density functional theory calculations: towards new NLO materials. Comput. Theor. Chem. 1133, 25–32 (2018)
- M. Khalid, M.N. Arshad, S. Murtaza, I. Shafiq, M. Haroon, A.M. Asiri, S.F. de Alcantara Moraise, A.A.C. Braga, Enriching



- NLO efficacy via designing non-fullerene molecules with the modification of acceptor moieties into ICIF2F: an emerging theoretical approach. RSC Adv. 12, 13412 (2022)
- B.-G. Kim, C.-G. Zhen, E.J. Jeong, J. Kieffer, J. Kim, Organic dye design tools for efficient photocurrent generation in dyesensitized solar cells: exciton binding energy and electron acceptors. Adv. Funct. Mater. 22, 1606–1612 (2012)
- A.M. Love, M.C. Cendejas, B. Thomas, W.P. McDermott, P. Uchupalanun, C. Kruszynski, S.P. Burt, T. Agbi, A.J. Rossini, I. Hermans, Synthesis and characterization of silica-supported boron oxide catalysts for the oxidative dehydrogenation of propane. J. Phys. Chem. C 123, 27000–27011 (2019)
- M. Rouhani, A detailed computational investigation on the structural and spectroscopic properties of propolisbenzofuran B. Heliyon 5, e02518 (2019)
- S. Dheivamalar, K. Bansura Banu, The adsorption mechanism, structural and electronic properties of pyrrole absorbed ZnO nano clusters in the field photovoltaic cells by density functional theory. Ind. J. Pure Appl. Phys. 57, 713–724 (2019)
- S. Khan, H. Sajid, K. Ayub, T. Mahmood, Sensing of toxic Lewisite (L1, L2, and L3) molecules by graphdiyne nanoflake using density functional theory calculations and quantum theory of atoms in molecule analysis. J. Phys. Org. Chem. 34, e4181 (2021)
- K. Tanaka, Y. Chujo, New idea for narrowing an energy gap by selective perturbation of one frontier molecular orbital. Chem. Lett. 50, 269–279 (2021)
- A. Migalska-Zalas, K. EL Korchi, T. Chtouki, Enhanced nonlinear optical properties due to electronic delocalization in conjugated benzodifuran derivatives. Opt. Quantum. Electron. 50, 389 (2018)
- 78. R. Karinzadeh, spatial self-phase modulation of a laser beam propagating through liquids with self-moduced natural convection flow. J. Opt. **149**, 095701 (2012)
- S.D. Durbin, S.M. Arakelian, Y.R. Shen, Laser-induced diffraction rings from a nematic-liquid-crystal film. Opt. Lett. 6, 411–413 (1981)
- K. Ogusu, Y. Kohtani, H. Shao, Laser- induced diffraction rings from an absorbing solution. Opt. Rev. 3, 232–234 (1993)
- B. Anusha, S. Jeyaram, Solvatochromism effect on third-order NLO properties of Azo dye. J. Opt. 53, 574–581 (2024)
- N.S. Arunsankar, S. Devanesan, M.S. AlSalhi, M. Vimalan,
 S. Jeyaram, Correction to: Nonlinear optical refraction and

- absorption features of methyl orange dye in polar solvents. J. Fluoresc. (2024). https://doi.org/10.1007/s10895-024-03636-6
- S. Jeyaram, Study of third-order NLO properties of organic dye for optoelectronics applications. Optoelectron. Adv. Mater. Rapid Commun. 15, 62–66 (2021)
- B. Anusha, N. Arumugam, A.I. Almansour, S. Jeyaram, A.G. Bharathi Dileepan, Polar solvents mediated third-order nonlinear optical features of acid green 16 dye. J. Opt. (2024). https://doi. org/10.1007/s12596-024-02146-9
- N.S. Arunsankar, A.G. Bharathi Dileepan, N. Arumugam, A.I. Almansour, S. Jeyaram, Study of solvent dependent on thirdorder nonlinear optical and thermo-optic coefficient of malachite green dye. J. Fluoresc. (2024). https://doi.org/10.1007/ s10895-024-03981-6
- K.A. Hussein, H.A. Sultan, A. Abdul-Radha, M. Aljaber, Q.M.A. Hassan, C.A. Emshary, Synthesis, characterization and nonlinear optical properties of new azo compound using CW laser beam. Opt. Quantum Electron. 56, 1056 (2024)
- K. Kumara, T.C.S. Shetty, S.R. Maidur, P.S. Patil, S.M. Dharmaprakash, Continuous wave laser induced nonlinear optical response of nitrogen doped graphene oxide. Optik 178, 384–393 (2019)
- S.R. Maidur, P.S. Patil, Linear optical and third-order nonlinear optical properties of anthracene chalcone derivatives doped PMMA thin films. Optik 190, 54–67 (2019)
- N.A. Raheem, Q.M.A. Hassan, A.M. Dhumad, H.A. Sultan, T. Fahad, C.A. Emshary, N.W. Ali, DFT structural and optical non-linear investigations of a synthesized new azo β-diketone dye. J. Ind. Chem. Soc. 100, 100928 (2023)
- M. Nadafan, M. Parishani, Z. Dehghania, J.Z. Anvari, R. Malekfar, Third-order nonlinear optical properties of NiFe2O4 nanoparticles by Z-scan technique. Optik 144, 672–678 (2017)

Publisher's Note Springer Nature remains neutral with regard to jurisdictional claims in published maps and institutional affiliations.

Springer Nature or its licensor (e.g. a society or other partner) holds exclusive rights to this article under a publishing agreement with the author(s) or other rightsholder(s); author self-archiving of the accepted manuscript version of this article is solely governed by the terms of such publishing agreement and applicable law.

